

Pattern formation of bulk-surface reaction-diffusion systems in a ball.

Edgardo Villar-Sepúlveda* Alan R. Champneys† Davide Cusseddu‡
 Anotida Madzvamuse§

Abstract

Weakly nonlinear amplitude equations are derived for the onset of spatially extended patterns on a general class of n -component bulk-surface reaction-diffusion systems in a ball, under the assumption of linear kinetics in the bulk. Linear analysis shows conditions under which various pattern modes can become unstable to either generalised pitchfork or transcritical bifurcations depending on the parity of the spatial wavenumber. Weakly nonlinear analysis is used to derive general expressions for the multi-component amplitude equations of different patterned states. These reduced-order systems are found to agree with prior normal forms for pattern formation bifurcations with $O(3)$ symmetry and provide information on the stability of bifurcating patterns of different symmetry types. The analysis is complemented with numerical results using a dedicated finite-element method. The theory is illustrated in two examples; a bulk-surface version of the Brusselator, and a four-component cell-polarity model.

1 Introduction

Recently, there have been substantial developments in extending the ground-breaking theory for pattern formation proposed by Alan Turing in his seminal paper in 1952 [51]; see for example [31] and references therein. One such development, driven primarily by experimental observations in biology and material science, is the formulation of bulk-surface reaction-diffusion models (BS-RDEs), see e.g [37, 38, 45, 46]. Here, a reaction-diffusion system is posed on two different, yet compatible geometries; one denoted the *bulk*, which describes the interior of the domain; and the *surface*, which describes the enclosing smooth manifold representing its boundary. These models naturally describe many biological and physical processes, such as symmetry-breaking and polarity formation in cell biology [10, 20, 21], surfactant dynamics [17, 26, 30], and spatiotemporal electrodeposition in batteries [27], to give just a few examples.

The complex coupled nature of such models tends to involve not only nonlinear reaction kinetics but also different spatial operators (Laplace and Laplace-Beltrami) for fields posed on the interior and boundary of the domain. The mathematical analysis of the resulting so-called bulk-surface partial differential equations is still in its infancy, and we do not attempt a full existence and uniqueness theory here. Instead, we conduct linear, weakly nonlinear, and numerical analysis of a general class bulk-surface reaction-diffusion systems (BS-RDSs) in 3D.

The class of BS-RDEs we consider consists of an arbitrary number $n \geq 2$ of components whose dynamics on the bulk and surface are coupled through linear mixed Robin (inhomogeneous Neumann) boundary conditions. Here, any analysis is greatly simplified if there is compatibility between the eigenfunctions of the ‘ground-state’ steady solution with respect to the Laplace and Laplace-Beltrami operators in the two different domains. The simplest geometries with natural compatibility are a circle in 2D (the bulk being the

*Department of Engineering Mathematics, University of Bristol, Bristol, UK (edgardo.villar-sepulveda@bristol.ac.uk).

†Department of Engineering Mathematics, University of Bristol, Bristol, UK (a.r.champneys@bristol.ac.uk).

‡CMAT – Centro de Matemática, Universidade do Minho, Braga, Portugal (davide.cusseddu@gmail.com).

§University of British Columbia, Department of Mathematics, 1984 Mathematics Road, Vancouver, V6T 1Z2, British Columbia, Canada; University of Pretoria and University of Johannesburg, Department of Mathematics, South Africa, and University of Zimbabwe, Department of Mathematics and Computational Science, Mt Pleasant, Harare, Zimbabwe (am823@math.ubc.ca, <https://www.math.ubc.ca/user/3665>).

interior of the circle, and the surface being its boundary) and a ball in 3D. We restrict the analysis here to the case of the ball with linear kinetics in the bulk, see Sec. 2 for more details.

The purpose of this study is to understand the nature of patterned states that can form under parameter variation, as a bifurcation from a trivial radially-symmetric ground state. One inspiration for the present work is due to Paquin-Lefebvre *et al* [42], who follow a similar procedure on a disk, where rotational symmetry is exploited to carry out the analysis. However, the case of a bulk-surface reaction-diffusion model posed on a ball is more complex due to the extra symmetries involved. See [16, 39, 40, 12] and references therein for analogous bifurcation results for reaction-diffusion systems posed on the surface of a sphere.

The main result (see Sec. 4) is to derive general expressions for amplitude equations for small-amplitude steady patterns that can be used to determine the bifurcation and stability of different patterned states. We find that these amplitude equations take the same form as those describing Turing bifurcations of PDE-systems posed on the surface of the sphere [12], owing to the underlying $O(3)$ symmetry of both problems.

We complement this analytical work with numerical solutions to the initial value problem to illustrate patterns emerging from the fully nonlinear system and to show their transient dynamics. These results are developed using a state-of-the-art finite element method for nonlinear semilinear parabolic partial differential equations (PDEs) of which BS-PDEs are one such class [6, 22, 23, 37, 38].

To illustrate our results, we choose two examples. One is a bulk-surface version of the well-studied Brusselator model [43] in which there is an activator and an inhibitor field. The other is a four-component system that is inspired by problems in cell biology, specifically the reaction-diffusion kinetics of small GTPases; these are key molecular proteins that exhibit co-localisation of their molecular concentrations and interactions in both the bulk and surface geometries as active and inactive species. See e.g. [7, 14] for a general introduction to models of such biological processes and [8, 20, 21, 49] for work on specific bulk-surface versions of them.

For each example, we identify bifurcation curves in a parameter plane, corresponding to instabilities of the ground state for different spatial wavenumbers. From there, we derive the normal forms and give predictions for the bifurcation and stability of different kinds of steady patterns. These are corroborated by numerical simulations, which also suggest the existence of more spatially localised patterns, that are at least meta-stable. However, for higher wavenumbers, the amplitude equations have many components, and their full analysis is unknown. A complete analysis of their spatiotemporal dynamics including the analogs of possible localised patterns after subcritical bifurcation (see e.g. [13, 9]), will be left for future work.

The rest of the article is structured as follows. In Section 2 we present the general class of BS-RDS, its linearised analysis together with the main result on how to construct the appropriate weakly nonlinear normal forms at pattern formation instabilities of different wavenumbers. The normal forms that arise have been analysed before in the context of systems with $O(3)$ symmetry, and we outline some of their dynamics in Section 3. The proof of the main result is contained in Section 4. Section 5 presents two examples where we show how the results of explicit computation of normal form coefficients explain what is observed in the finite-element simulations. Finally, Section 6 contains concluding remarks and suggests avenues for future work.

2 General theory

We consider a general class of BS-RDSs posed in a ball of radius $R > 0$. For analytical purposes, we restrict the class of PDEs in the bulk to be linear. We then find a general expression for its ground state and categorise its spectrum using modified spherical Bessel functions and associated Legendre polynomials. This leads to a statement of our main result, which is to provide closed-form expressions for the amplitude equations valid in a neighbourhood of pattern formation bifurcations for different wavenumbers.

2.1 A class of bulk-surface reaction-diffusion systems in a ball

Consider the ball $\Omega = \{\mathbf{x} \in \mathbb{R}^3 : \|\mathbf{x}\| \leq R\}$ which we refer to as the *bulk* domain; its boundary $\Gamma = \partial\Omega = \{\mathbf{x} \in \mathbb{R}^3 : \|\mathbf{x}\| = R\}$ will be called the *surface*. Consider an n -component field of spatiotemporal unknowns, designating its bulk components using capital letters, $U_1, \dots, U_n : \Omega \times \mathbb{R}_0^+ \rightarrow \mathbb{R}$, and surface components using lowercase letters $u_1, \dots, u_n : \Gamma \times \mathbb{R}_0^+ \rightarrow \mathbb{R}$. In compact form, suppose $\mathbf{U} = (U_1, \dots, U_n)^\top$ and $\mathbf{u} =$

$(u_1, \dots, u_n)^\top$ satisfy the following system

$$\begin{cases} \partial_t \mathbf{U} = -B \mathbf{U} + \mathbb{D}_U \nabla_\Omega^2 \mathbf{U}, & \text{in } \Omega, \\ \mathbb{D}_U \frac{\partial \mathbf{U}}{\partial \hat{\mathbf{n}}} = K(\mathbf{u} - \mathbf{U}|_\Gamma), & \text{on } \Gamma, \\ \partial_t \mathbf{u} = \mathbf{g}(\mathbf{u}) - K(\mathbf{u} - \mathbf{U}|_\Gamma) + \mathbb{D}_u \nabla_\Gamma^2 \mathbf{u}, & \text{on } \Gamma, \end{cases} \quad (1)$$

where $B = \text{diag}(\sigma_1, \dots, \sigma_n) \in (\mathbb{R}_0^+)^{n \times n}$, $K = \text{diag}(K_1, \dots, K_n) \in (\mathbb{R}_0^+)^{n \times n}$, $\mathbf{g} : \mathbb{R}^n \rightarrow \mathbb{R}^n$ is a \mathcal{C}^3 nonlinear vector function, $\hat{\mathbf{n}}$ is the outward unit vector to Ω on Γ , $\mathbb{D}_U = \text{diag}(D_1, \dots, D_n)$, and $\mathbb{D}_u = \text{diag}(d_1, \dots, d_n)$. We allow B , \mathbb{D}_U , K , and \mathbf{g} to depend on a parameter, μ , defined as the unfolding parameter in the sequel. For simplicity, we omit the parameter dependence of these functions. Note that the presence of the same factor $K(\mathbf{u} - \mathbf{U}|_\Gamma)$ in the 2nd and 3rd equations of (1) leads to consistent Langmuir boundary conditions (*cf.* [42]), which couple bulk and surface fields.

2.2 The ground state and linearisation about it

We seek a radially-symmetric steady state for the coupled system as follows: let $r = \|\mathbf{x}\|$, and consider a solution $\mathbf{P} = (\mathbf{U}^*, \mathbf{u}^*)^\top = (\mathbf{U}^*(r), \mathbf{u}^*)^\top$ of the system such that $\partial_t \mathbf{U}^* = \mathbf{0}$ and $\partial_t \mathbf{u}^* = \mathbf{0}$. In particular, passing to spherical coordinates, $\mathbf{U}^*(r)$ must satisfy

$$r^2 \frac{\partial^2 \mathbf{U}^*}{\partial r^2} + 2r \frac{\partial \mathbf{U}^*}{\partial r} - r^2 \mathbb{D}_U^{-1} B \mathbf{U}^* = \mathbf{0}, \quad \text{for } r \in (0, R). \quad (2)$$

We seek a solution to (2) of the form $\mathbf{U}^* = i_0(\boldsymbol{\omega} r) \mathbf{U}^\dagger$, where $\mathbf{U}^\dagger \in \mathbb{R}^n$ is a constant vector, $\boldsymbol{\omega} = \text{diag}(\omega_1, \dots, \omega_n)$, with $\omega_p = \sqrt{\sigma_p/D_p}$, for $p = 1, \dots, n$, and $i_0(\boldsymbol{\omega} r) = \text{diag}(i_0(\omega_1 r), \dots, i_0(\omega_n r))$, where i_0 is a modified spherical Bessel function of the first kind [2, eq. 10.2.12].

To determine \mathbf{U}^\dagger and \mathbf{u}^* , we use the boundary conditions (the 2nd equation of (1)). Thus, we obtain $\mathbb{D}_U i_0'(\boldsymbol{\omega} R) \boldsymbol{\omega} \mathbf{U}^\dagger = K(\mathbf{u}^* - i_0(\boldsymbol{\omega} R) \mathbf{U}^\dagger)$, which can be rearranged into the form

$$\mathbf{U}^\dagger = S_0 \mathbf{u}^*, \quad \text{where } S_0 := (\mathbb{D}_U i_0'(\boldsymbol{\omega} R) \boldsymbol{\omega} + K i_0(\boldsymbol{\omega} R))^{-1} K. \quad (3)$$

Here, we use $i_0'(\boldsymbol{\omega} r)$ to denote the diagonal matrix with entries $i_0'(\omega_p r)$, $p = 1, \dots, n$, and a prime means differentiation with respect to r .

Finally, we use the third equation of (1) to obtain:

$$\mathbf{g}(\mathbf{u}^*) - K(I - i_0(\boldsymbol{\omega} R) S_0) \mathbf{u}^* = \mathbf{0}, \quad (4)$$

where I is the identity matrix of size $n \times n$. Therefore, a radially-symmetric steady state of the form $\mathbf{P} = (\mathbf{U}^*(r), \mathbf{u}^*)^\top$ can be found whenever there is a solution \mathbf{u}^* to (4), by setting $\mathbf{U}^* = i_0(\boldsymbol{\omega} r) S_0 \mathbf{u}^*$, with S_0 given by (3).

Now, let $J_{\mathbf{u}} \mathbf{f}(\mathbf{P})$ denote the Jacobian matrix of (1) at \mathbf{P} in the absence of diffusion, i.e., $J_{\mathbf{u}} \mathbf{f}(\mathbf{P}) = \begin{pmatrix} -B & \mathbf{0}_{n \times n} \\ K \mathbb{I}|_\Gamma & -K + J_{\mathbf{u}} \mathbf{g}(\mathbf{u}^*) \end{pmatrix}$. Here, $J_{\mathbf{u}} \mathbf{g}(\mathbf{u}^*)$ denotes the Jacobian matrix of \mathbf{g} at \mathbf{u}^* and $\mathbb{I}|_\Gamma$ means restriction onto Γ such that $\mathbb{I}|_\Gamma(\mathbf{U}) = \mathbf{U}|_\Gamma$. Also, let \mathbb{D} denote the diffusion matrix of (1) given by $\mathbb{D} = \begin{pmatrix} \mathbb{D}_U & \mathbf{0}_{n \times n} \\ \mathbf{0}_{n \times n} & \mathbb{D}_u \end{pmatrix}$. This implies that the Jacobian matrix of the full system at \mathbf{P} is given by $J_{\mathbf{u}} \mathbf{f}(\mathbf{P}) + \mathbb{D} \nabla^2$, where $\nabla^2 = (\nabla_\Omega^2, \nabla_\Gamma^2)^\top$.

In what follows, we shall be interested in bifurcations of this ground state. In such analysis, we are mostly interested in the kernel of the linear equation. Thus, the problem becomes more or less equivalent to the bifurcation problem for reaction-diffusion systems on the sphere with a constant steady state \mathbf{u}^* , albeit influenced by the linear equation in the bulk. Hence, we are interested in the space of eigenfunctions of the operator ∇^2 , which satisfy

$$\nabla_\Omega^2 \mathbf{U}(r, \theta, \phi) = -k^2 \mathbf{U}(r, \theta, \phi), \quad \text{and} \quad \nabla_\Gamma^2 \mathbf{u}(\theta, \phi) = -\frac{\ell(\ell+1)}{R^2} \mathbf{u}(\theta, \phi), \quad (5)$$

with eigenvalues $-k^2$ and $-\ell(\ell+1)/R^2$ in the bulk and on the sphere, respectively. Specifically, we find that the eigenfunctions satisfy

$$\begin{pmatrix} \mathbf{U}(r, \theta, \phi) \\ \mathbf{u}(\theta, \phi) \end{pmatrix} = Y_\ell^m(\theta, \phi) \begin{pmatrix} j_\ell(kr) \hat{\boldsymbol{\varphi}} \\ \boldsymbol{\varphi} \end{pmatrix}, \quad (6)$$

where $Y_\ell^m(\theta, \phi) = P_\ell^m(\cos(\theta)) e^{im\phi}$, j_ℓ is a spherical Bessel function of the first kind, P_ℓ^m is an associated Legendre polynomial (normalized as in [29, eqns. (2.1.20-21)] so that $\int_{-1}^1 (P_\ell^m(x))^2 dx = 1$, and $\hat{\boldsymbol{\varphi}}, \boldsymbol{\varphi} \in \mathbb{R}^n$ are constant vectors [19].

Now, based on the approach used in [24, 42] to develop amplitude equations for steady solutions, we consider perturbations to the ground state of the form

$$\begin{pmatrix} \mathbf{U} \\ \mathbf{u} \end{pmatrix} = \mathbf{P} + \sum_{m=-\ell}^{\ell} A_m \begin{pmatrix} i_\ell(\omega r) \hat{\boldsymbol{\varphi}} \\ \boldsymbol{\varphi} \end{pmatrix} Y_\ell^m(\theta, \phi) \quad (7)$$

where $A_m = A_m(t) \in \mathbb{C}$ is a complex variable such that $A_{-m} = (-1)^m \overline{A_m}$ for each $-\ell \leq m \leq \ell$.

2.3 The main result

As is common for bifurcation problems on a sphere [18, 12, 40], we shall find that odd (respectively, even) values of ℓ give rise to pitchfork (respectively, transcritical) pattern-formation bifurcations for the amplitudes of the bulk-surface system (1). We shall now formalise this result, and give expressions for amplitude equations we get at each bifurcation in terms of the coefficients of the underlying system. It is convenient to introduce some notation. For each non-negative integer (wavenumber) ℓ , we define the matrix

$$\mathbb{B}_\ell := K(i_\ell(\omega R) S_\ell - I) + J_{\mathbf{u}} \mathbf{g}(\mathbf{u}^*) - \frac{\ell(\ell+1)}{R^2} \mathbb{D}_{\mathbf{u}}, \quad (8)$$

where $S_\ell := (\mathbb{D}_U i'_\ell(\omega R) \boldsymbol{\omega} + K i_\ell(\omega R))^{-1} K$. Moreover, we introduce the following multilinear symmetric vector functions:

$$\mathbf{G}_{1,1}(\mathbf{a}) = \left(\sum_{p=1}^n a_p \frac{\partial}{\partial \mu} \left(\frac{\partial g_j}{\partial u_p}(\mathbf{u}^*(\mu), \mu) \right) \Big|_{\mu=\mu^*} \right)_{1 \leq j \leq n}, \quad (9)$$

$$\mathbf{G}_2(\mathbf{a}, \mathbf{b}) = \frac{1}{2} \left(\sum_{1 \leq p, q \leq n} a_p b_q \frac{\partial^2 g_j}{\partial u_p \partial u_q}(\mathbf{u}^*) \right)_{1 \leq j \leq n}, \quad (10)$$

$$\mathbf{G}_3(\mathbf{a}, \mathbf{b}, \mathbf{c}) = \frac{1}{6} \left(\sum_{1 \leq p, q, s \leq n} a_p b_q c_s \frac{\partial^3 g_j}{\partial u_p \partial u_q \partial u_s}(\mathbf{u}^*) \right)_{1 \leq j \leq n}, \quad (11)$$

where $\mathbf{g} = (g_1, \dots, g_n)$, $\mathbf{a} = (a_1, \dots, a_n)^\top \in \mathbb{R}^n$, $\mathbf{b} = (b_1, \dots, b_n)^\top \in \mathbb{R}^n$, $\mathbf{c} = (c_1, \dots, c_n)^\top \in \mathbb{R}^n$, and $\mu^* \in \mathbb{R}$. The main result of this study can be stated as follows:

Theorem 1. *Let $\mathbf{P} = (\mathbf{U}^*(r), \mathbf{u}^*)^\top$ be a radially-symmetric steady state of (1) and $\mathbb{B}_\ell, \mathbf{G}_{1,1}, \mathbf{G}_2, \mathbf{G}_3$ as defined in (8)-(11). If there exists $\mu^* \in \mathbb{R}$ and a critical wavenumber ℓ such that*

$$\det(\mathbb{B}_\ell) = 0, \quad \ker(\mathbb{B}_\ell) \cap \text{Im}(\mathbb{B}_\ell) = \{\mathbf{0}\}, \quad \text{and} \quad C_{1,1} \neq 0, \quad (12)$$

where

$$\begin{aligned} C_{1,1} = & \frac{1}{I_\ell} \left(\int_0^R \left(-\frac{\partial B}{\partial \mu} i_\ell(\omega r) S_\ell \boldsymbol{\varphi} \right) \cdot (i_\ell(\omega r) S_\ell \boldsymbol{\psi}) r^2 dr \right. \\ & \left. + R^2 \left(\mathbf{G}_{1,1}(\boldsymbol{\varphi}) - \frac{\partial K}{\partial \mu} (\boldsymbol{\varphi} - i_\ell(\omega R) \hat{\boldsymbol{\varphi}}) \right) \cdot \boldsymbol{\psi} \right) \end{aligned}$$

$$-\frac{\ell(\ell+1)}{R^2} \left(\int_0^R \left(\frac{\partial \mathbb{D}_U}{\partial \mu} i_\ell(\omega r) S_\ell \varphi \right) \cdot (i_\ell(\omega r) S_\ell \psi) r^2 dr + R^2 \left(\frac{\partial \mathbb{D}_u}{\partial \mu} \varphi \right) \cdot \psi \right), \quad (13)$$

$$I_\ell = \int_0^R i_\ell(\omega r) S_\ell \varphi \cdot i_\ell(\omega r) S_\ell \psi r^2 dr + R^2 \varphi \cdot \psi,$$

with $\varphi \in \ker(\mathbb{B}_\ell) \setminus \{\mathbf{0}\}$ and $\psi \in \ker(\mathbb{B}_\ell^T) \setminus \{\mathbf{0}\}$, then

1. If ℓ is even, and the quadratic coefficients of the amplitude equations (15) are different from zero, then the system undergoes a codimension-one (Turing) transcritical bifurcation as μ varies through μ^* .
2. If ℓ is even and the quadratic coefficients of the amplitude equations (15) are equal to zero, then the system undergoes a codimension-two (Turing) transcritical bifurcation as μ varies through μ^* .
3. If ℓ is odd, and $\det(\mathbb{B}_p) \neq 0$ for every even integer $0 \leq p \leq 2\ell$, then the system undergoes a (Turing) pitchfork bifurcation as μ varies through μ^* .

Furthermore, all of these bifurcations are described by a vector \mathbf{A} of $2\ell+1$ amplitudes that fulfill the following:

1. If ℓ is even and the quadratic coefficients of the amplitude equations (15) are different from zero, then

$$\dot{A}_m = C_{1,1} (\mu - \mu^*) A_m + \sum_{\substack{-\ell \leq q_1 \leq q_2 \leq \ell \\ q_1 + q_2 = m}} C_{q_1, q_2, m}^{[2]} A_{q_1} A_{q_2} + \mathcal{O}(\|\mathbf{A}\|^3), \quad (14)$$

for each $m \in [-\ell, \ell] \cap \mathbb{Z}$, where

$$C_{q_1, q_2, m}^{[2]} = \frac{R^2}{I_\ell} \delta_{m, q_1 + q_2} d_{\ell, q_1, q_2}^{[2]} \mathbf{G}_2(\varphi, \varphi) \cdot \psi, \quad (15)$$

and $\delta_{m, q_1 + q_2}$ is the Kronecker delta function that is equal to 1 if $m = q_1 + q_2$ and 0 otherwise.

2. If ℓ is odd or ℓ is even and the quadratic coefficients of the amplitude equations (15) are equal to zero, then

$$\dot{A}_m = C_{1,1} (\mu - \mu^*) A_m + \sum_{\substack{-\ell \leq q_1 \leq q_2 \leq q_3 \leq \ell \\ q_1 + q_2 + q_3 = m}} C_{q_1, q_2, q_3, m}^{[3]} A_{q_1} A_{q_2} A_{q_3} + \mathcal{O}(\|\mathbf{A}\|^4), \quad (16)$$

for each $m \in [-\ell, \ell] \cap \mathbb{Z}$, where

$$C_{q_1, q_2, q_3, m}^{[3]} = \frac{R^2}{I_\ell} \delta_{m, q_1 + q_2 + q_3} \left(2 \sum_{p=|q_1 + q_2|}^{2\ell} \tilde{d}_{p, q_1, q_2}^{[2]} \mathbf{G}_2(\mathbf{u}_{p, q_1, q_2}^{[2]}, \varphi) \cdot \psi + \tilde{d}_{q_1, q_2, q_3}^{[3]} \mathbf{G}_3(\varphi, \varphi, \varphi) \cdot \psi \right),$$

with

$$\tilde{d}_{p, q_1, q_2}^{[2]} = \int_{-1}^1 P_\ell^{q_3}(x) P_p^{q_1 + q_2}(x) P_\ell^m(x) dx,$$

$$\tilde{d}_{q_1, q_2, q_3}^{[3]} = \int_{-1}^1 P_\ell^{q_1}(x) P_\ell^{q_2}(x) P_\ell^{q_3}(x) P_\ell^m(x) dx,$$

and $\mathbf{u}_{p, q_1, q_2}^{[2]}$ solves

$$\mathbb{B}_p \mathbf{u}_{p, q_1, q_2}^{[2]} = -d_{p, q_1, q_2}^{[2]} \mathbf{G}_2(\varphi, \varphi), \quad \text{with}$$

$$d_{p, q_1, q_2}^{[2]} = \int_{-1}^1 P_\ell^{q_1}(x) P_\ell^{q_2}(x) P_p^{q_1 + q_2}(x) dx,$$

for each set of integers $-\ell \leq p, m, q_1, q_2, q_3 \leq \ell$.

In the above, all the coefficients $C_{1,1}$, $C_{q_1, q_2, m}^{[2]}$, $C_{q_1, q_2, q_3, m}^{[3]}$ are evaluated at $\mu = \mu^*$.

The proof of Theorem 1 is contained in Section 4.

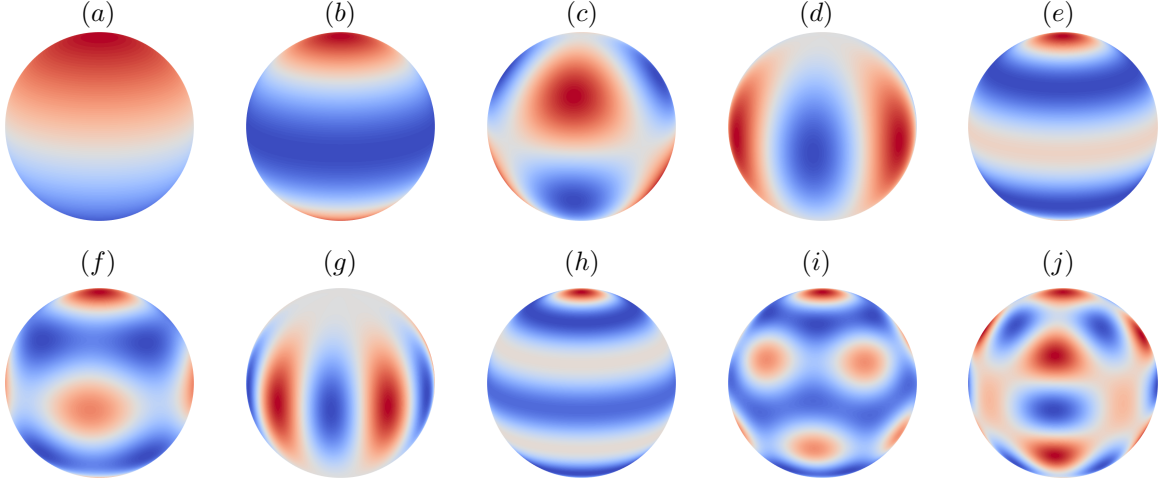


Figure 1: A collection of spherical harmonics and some of their linear combinations. Top row, from left to right: $Y_1^0(\theta, \phi)$, $Y_2^0(\theta, \phi)$, $Y_3^0(\theta, \phi)$, $Y_4^0(\theta, \phi)$, $Y_5^0(\theta, \phi)$. Bottom row, from left to right: $\sqrt{14}Y_4^0(\theta, \phi) + \sqrt{5}Y_4^4(\theta, \phi)$, $Y_5^5(\theta, \phi)$, $Y_6^0(\theta, \phi)$, $\sqrt{11}Y_6^0(\theta, \phi) + \sqrt{7}Y_6^5(\theta, \phi)$, $\sqrt{2}Y_6^0(\theta, \phi) + \sqrt{7}Y_6^4(\theta, \phi)$. These functions are reported in Figure 1 of [12], respectively as Solution 1, 2, 4, 5, 6, 7, 9, 16, 17, and 18.

3 The dynamics of the normal forms

Equations (14) and (16) have precisely the same form as the normal forms derived for Turing bifurcations in systems with $O(3)$ -symmetry. We note that such normal forms were previously derived for PDEs posed on the surface of a sphere. Here, we show that we get the same expressions for the bulk-surface case. In particular, Callahan [12] (see also the earlier results by Chossat *et al* [18]) has shown how the coefficients of the normal forms for different values of ℓ are consequent on the symmetry of the problem. From this, he was able to apply the equivariant branching Lemma [28] to find the criticality (direction of bifurcation curves) and stability of each different kind of bifurcating pattern up to $\ell = 6$. This leads to the conjecture in [12] that only 10 topologically distinct stable steady patterns can arise for $\ell \leq 6$; see Fig. 1. Other information is available in [39, 40] for higher ℓ including numerical indications of complex spatio-temporal dynamics. Nevertheless, a full investigation of the dynamics of the normal forms, even for the lowest values of ℓ is, as far as we are aware, unknown. We summarise here, for use later on when we compute examples, some basic results for low values of ℓ , highlighting what remains to be investigated.

3.1 The case $\ell = 1$

Here, $2\ell + 1 = 3$, so there are three coordinates in the amplitude vector $\mathbf{A} = (A_{-1}, A_0, A_1)^\top$, such that, as in definition (7), $A_{-1} = -\overline{A_1}$. Following the theory developed in [12], we expect to find the specific form of the amplitude equations:

$$\begin{cases} \dot{A}_0 = A_0 (\varepsilon + a A_0^2 - 2a A_{-1} A_1) + \mathcal{O}(\|\mathbf{A}\|^4), \\ \dot{A}_1 = A_1 (\varepsilon + a A_0^2 - 2a A_{-1} A_1) + \mathcal{O}(\|\mathbf{A}\|^4), \end{cases} \quad (17)$$

with the conjugate equation for A_{-1} . Here, there are two real parameters to be determined, a single criticality coefficient $a \in \mathbb{R}$ and an unfolding parameter $\varepsilon = C_{1,1}(\mu - \mu^*)$, defined so that the origin is stable whenever $\varepsilon < 0$.

Neglecting higher-order terms, (17) has a family of steady states defined by $A_0 = A_1 = A_{-1} = 0$ and $\varepsilon + a A_0^2 - 2a A_{-1} A_1 = 0$, and at least two invariant subspaces given by $A_0 = 0$, and $A_{-1} = A_1 = 0$. Only the latter is analyzed carefully in [12], referred to as the ‘primary branch’. However, the former is also an invariant manifold and, when $A_0 = 0$, (17) becomes $\dot{A}_1 = A_1 (\varepsilon + 2a |A_1|^2)$, whilst when $A_{-1} = A_1 = 0$, (17)

becomes $\dot{A}_0 = A_0 (\varepsilon + a A_0^2)$. These systems are the normal forms of simple rotational pitchfork bifurcations which turn out to be supercritical (resp. subcritical) if and only if the third-order coefficient is negative (resp. positive) (see e.g. [50]).

On the other hand, looking at the structure of (17), even for the planar reduction in which $A_{-1} = -\overline{A_1}$, we have a one-dimensional continuum of steady states given by $\varepsilon + a A_0^2 - 2a A_{-1} A_1 = 0$. To analyze stability of this family, let $z = \varepsilon + a A_0^2 - 2a A_{-1} A_1 = \varepsilon + a A_0^2 + 2a |A_1|^2$. Therefore,

$$\begin{aligned} \dot{z} &= 2a A_0 \dot{A}_0 - 2a (\dot{A}_{-1} A_1 + A_{-1} \dot{A}_1) = 2a z (A_0^2 + 2|A_1|^2) + \mathcal{O}(\|\mathbf{A}\|^5) \\ &= 2z(z - \varepsilon) + \mathcal{O}(\|\mathbf{A}\|^5). \end{aligned}$$

Therefore, this family of steady states is stable for $\varepsilon > 0$, when the origin is unstable, but has a small basin of attraction in the direction of positive z . Thus, the full dynamics of (17) appears to be non-trivial.

3.2 The case $\ell = 2$

We now have $2\ell + 1 = 5$ components in the amplitude vector $\mathbf{A} = (A_{-2}, A_{-1}, A_0, A_1, A_2)^\top$, with $A_{-1} = -\overline{A_1}$, and $A_{-2} = \overline{A_2}$. Again, by the theory developed in [12], the amplitude equations should have the form

$$\begin{cases} \dot{A}_0 = A_0 (\varepsilon - 2a A_0) + 2a A_{-1} A_1 + 4a A_{-2} A_2 + A_0 \mathcal{P}_2(\mathbf{A}) + \mathcal{O}(\|A\|^4), \\ \dot{A}_1 = A_1 (\varepsilon - 2a A_0) + 2\sqrt{6}a A_{-1} A_2 + A_1 \mathcal{P}_2(\mathbf{A}) + \mathcal{O}(\|A\|^4), \\ \dot{A}_2 = A_2 (\varepsilon + 4a A_0) - \sqrt{6}a A_1^2 + A_2 \mathcal{P}_2(\mathbf{A}) + \mathcal{O}(\|A\|^4), \end{cases} \quad (18)$$

where $\mathcal{P}_2(\mathbf{A}) = -bA_0^2 + 2bA_{-1}A_1 - 2bA_{-2}A_2$, in addition to the conjugate equations for A_{-1} and A_{-2} . The equations now depend on two criticality parameters $a, b \in \mathbb{R}$, apart from the unfolding parameter ε . Finding all invariant subspaces is trickier than (17). However, some general results can still be obtained.

Lemma 1. *When neglecting cubic and higher-order terms in (18), the following are invariant subspaces*

$$A_{-1} = A_1 = 0 \quad \text{and} \quad |A_2|^2 = \frac{3}{2} A_0^2, \quad (19)$$

$$A_0 = 0 \quad \text{and} \quad |A_1|^2 = 2|A_2|^2, \quad (20)$$

while

$$\begin{aligned} 4A_0 \left(-A_0 + \frac{\varepsilon}{a} \right) + 24|A_2|^2 = \frac{\varepsilon^2}{a^2}, \quad 2A_0 \left(4A_0 - \frac{\varepsilon}{a} \right) + 12|A_1|^2 = \frac{\varepsilon^2}{a^2}, \\ \text{and} \quad A_2 (\varepsilon + 4a A_0) - \sqrt{6}a A_1^2 = 0 \end{aligned} \quad (21)$$

give a manifold composed of steady states of (18).

The proof of this lemma is given in the Supplementary Materials A.

Rather than consider the full implications of these invariant manifolds, we can focus on the existence and stability of ‘primary’ steady states. Setting $A_1 = A_2 = 0$ in System (18), we have $\dot{A}_0 = A_0 (\varepsilon - 2a A_0 - b A_0^2)$. Thus, nontrivial states are given by $A_{0,\pm} = \frac{-a \pm \sqrt{a^2 + b\varepsilon}}{b}$. Now, we can easily delineate stability, based on the signs of a and b [12]. If $b < 0$ there is no stable small-amplitude pattern. If $b > 0$, then either $A_{0,+}$ or $A_{0,-}$ emerges stably from the bifurcation point, according to whether $a < 0$ or $a > 0$, respectively. See Figure 2.

3.3 The case $\ell = 3$

Here, there are $2\ell + 1 = 7$ components in the amplitude vector $\mathbf{A} = (A_{-3}, A_{-2}, A_{-1}, A_0, A_1, A_2, A_3)^\top$, with $A_{-3} = -\overline{A_3}$, $A_{-2} = \overline{A_2}$, and $A_{-1} = -\overline{A_1}$. Furthermore, in accordance with the theory developed in [18,

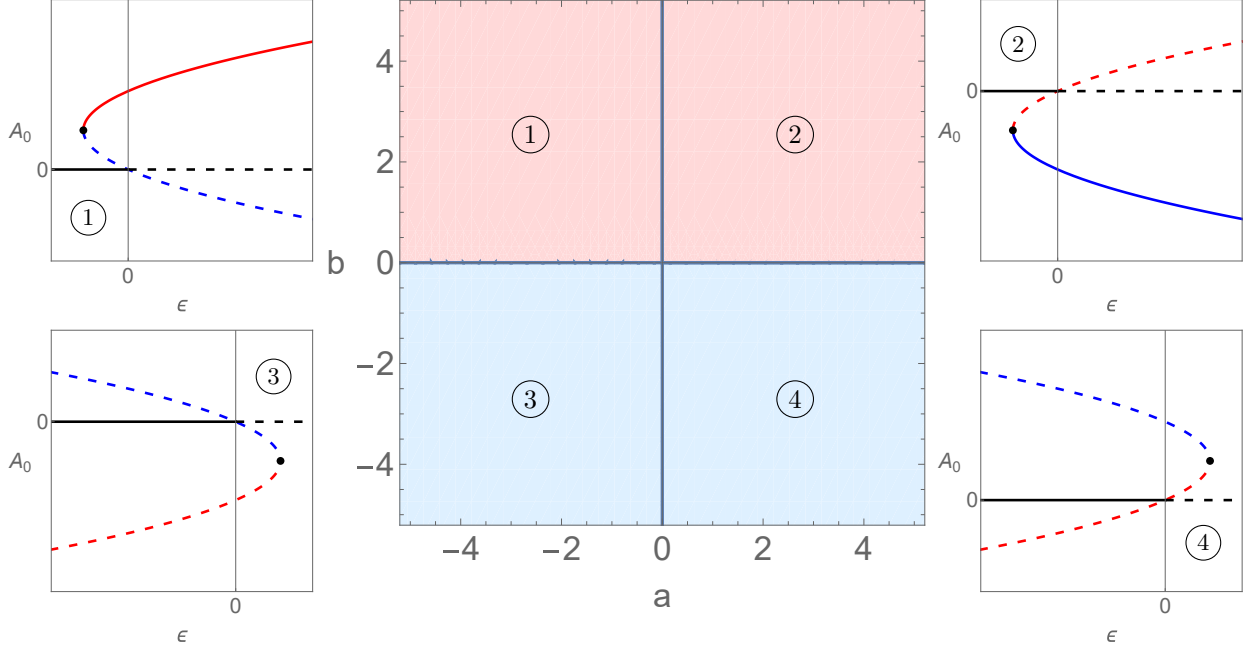


Figure 2: Partial bifurcation diagram for the transcritical bifurcation of the origin of the normal form (18) that arises when $\ell = 2$. Blue (respectively red) curves represent $A_{0,-}$ (resp. $A_{0,+}$). Moreover, dashed (resp. continuous) lines represent unstable (resp. stable) steady states.

Table B.2] (with the correction of typos in the coefficients of $A_{-2}A_1^2$ and $A_{-2}A_0A_3$ reported in [12]) we expect the amplitude equations to take the form

$$\begin{aligned}
\dot{A}_0 &= A_0 \left(\varepsilon + (-18a + b) A_0^2 + (36a - 2b) A_{-1} A_1 \right. \\
&\quad \left. + (-60a + 2b) A_{-2} A_2 - 2b A_{-3} A_3 \right) + 15\sqrt{2}a (A_{-3} A_1 A_2 + A_{-2} A_{-1} A_3) \\
&\quad + \sqrt{30}a (A_{-2} A_1^2 + A_{-1}^2 A_2) + \mathcal{O}(\|\mathbf{A}\|^4), \\
\dot{A}_1 &= A_1 \left(\varepsilon + (-18a + b) A_0^2 + (41a - 2b) A_{-1} A_1 + (-35a + 2b) A_{-2} A_2 \right. \\
&\quad \left. + (15a - 2b) A_{-3} A_3 \right) + 5\sqrt{15}a A_{-3} A_2 A_2 - 15\sqrt{2}a A_{-2} A_0 A_3 \\
&\quad + 6\sqrt{15}a A_{-1}^2 A_3 - 2\sqrt{30}a A_{-1} A_0 A_2 + \mathcal{O}(\|\mathbf{A}\|^4), \\
\dot{A}_2 &= A_2 \left(\varepsilon + (-30a + b) A_0^2 + (35a - 2b) A_{-1} A_1 + (-20a + 2b) A_{-2} A_2 \right. \\
&\quad \left. + (45a - 2b) A_{-3} A_3 \right) + \sqrt{30}a A_0 A_1^2 + 15\sqrt{2}a A_{-1} A_0 A_3 \\
&\quad - 10\sqrt{15}a A_{-2} A_1 A_3 + \mathcal{O}(\|\mathbf{A}\|^4), \\
\dot{A}_3 &= A_3 \left(\varepsilon + b A_0^2 + (15a - 2b) A_{-1} A_1 + (-45a + 2b) A_{-2} A_2 \right. \\
&\quad \left. + (45a - 2b) A_{-3} A_3 \right) + 5\sqrt{15}a A_{-1} A_2^2 - 15\sqrt{2}a A_0 A_1 A_2 \\
&\quad + 2\sqrt{15}a A_1^3 + \mathcal{O}(\|\mathbf{A}\|^4).
\end{aligned} \tag{22}$$

We now have two cubic parameters $a, b \in \mathbb{R}$, in addition to the unfolding parameter ε . In [12, 18], analysis can be found for some particular bifurcation branches according to different symmetry subgroups of $O(3)$. Specifically, according to the theory developed by these authors, three steady states become relevant to study. Those are the ones that follow $O(2)^-$, \mathbf{O} , and D_6^d symmetries, which correspond to the cases in which $A_{-3} = A_{-2} = A_{-1} = A_1 = A_2 = A_3 = 0$, $A_{-3} = A_{-1} = A_0 = A_1 = A_3 = 0$, and $A_{-2} = A_{-1} = A_0 = A_1 = A_2 = 0$, respectively [12]. These steady states are defined, respectively, by $\varepsilon = (18a - b) A_0^2$, $\varepsilon = 2(10a - b) A_{-1} A_1$, and $\varepsilon = (45a - 2b) A_{-3} A_3$. Furthermore, the steady-state associated with the

symmetry $O(2)^-$ is always unstable, whilst the second one can be stable only if $10a - b > 0$, and $a > 0$. Last but not least, the third one bifurcates stably only if $45a - 2b > 0$, and $a < 0$. Figure 3 shows the different regions one can find depending on the values of a and b in Equation (22). Clearly, the full nonlinear dynamics of the 7-dimensional normal form is likely to be somewhat complicated.

3.4 The case $\ell \geq 4$

When $\ell \geq 4$, we have that the amplitude vector has $2\ell + 1$ components, $\mathbf{A} = (A_{-\ell}, A_{-\ell+1}, \dots, A_{-1}, A_0, A_1, \dots, A_{\ell-1}, A_\ell)^\top$, with $A_{-j} = (-1)^j \bar{A}_j$, for each $j \in \{-\ell, -\ell+1, \dots, -1, 0, 1, \dots, \ell-1, \ell\}$, which requires analysis of dynamics in a $2\ell + 1$ -dimensional phase space.

For the specific case $\ell = 4$, even just up quadratic terms we have

$$\begin{cases} \dot{A}_0 = A_0 (\varepsilon - 18a A_0) + 18a A_{-1} A_1 + 22a A_{-2} A_2 \\ \quad - 42a A_{-3} A_3 - 28a A_{-4} A_4 + \mathcal{O}(\|\mathbf{A}\|^3), \\ \dot{A}_1 = A_1 (\varepsilon - 18a A_0) + 12\sqrt{10}a A_{-1} A_2 \\ \quad - 2\sqrt{70}a A_{-2} A_3 - 14\sqrt{10}a A_{-3} A_4 + \mathcal{O}(\|\mathbf{A}\|^3), \\ \dot{A}_2 = A_2 (\varepsilon + 22a A_0) - 6\sqrt{10}a A_1^2 \\ \quad + 2\sqrt{70}a A_{-1} A_3 - 6\sqrt{70}a A_{-2} A_4 + \mathcal{O}(\|\mathbf{A}\|^3), \\ \dot{A}_3 = A_3 (\varepsilon + 42a A_0) - 14\sqrt{10}a A_{-1} A_4 - 2\sqrt{70}a A_1 A_2 + \mathcal{O}(\|\mathbf{A}\|^3), \\ \dot{A}_4 = A_4 (\varepsilon - 28a A_0) + 14\sqrt{10}a A_1 A_3 - 3\sqrt{70}a A_2^2 + \mathcal{O}(\|\mathbf{A}\|^3). \end{cases} \quad (23)$$

The full equations up to and including cubic terms are given in the Supplementary Materials, where the cubic terms depend on two real parameters, b and c . Again, a complete analysis of such a 9-dimensional normal form is beyond the scope of this article.

Callahan [12] goes further, and supplies expressions for all the coefficients up to $\ell = 6$. He also establishes the general principles for deciding which steady states can bifurcate stably. Figure 1 shows the only primary steady states that Callahan argues can be stable for low amplitude, up to $\ell = 6$. The stability of these patterns depends explicitly on the values of the normal form coefficients, for which he derives specific conditions. In addition, Matthews [39, 40] finds explicit conditions for certain dihedral-symmetry states with large ℓ to bifurcate stably.

It is important here to understand one consequence of Theorem 1 (as already shown in the context of $O(3)$ -equivariant bifurcation theory in [40]); when ℓ is even and the second-order coefficients are different from zero, we need only to compute one scalar to obtain the leading-order unfolding of the transcritical bifurcation. On the other hand, when the second-order coefficients are zero, independently of the parity of ℓ , the cubic terms depend on $\lfloor \ell/3 \rfloor + 1$ independent coefficients that must be computed to determine the unfolding of the pitchfork bifurcation [18, 12]. The main contribution of the theorem is to derive expressions that enable us to compute such coefficients explicitly for the class of BS-RDEs considered here, and thus make predictions about which small-amplitude patterns should appear under parameter variation.

4 Calculation of the amplitude equations

We provide a proof of Theorem 1 using the method introduced by Elphick *et al* [24]. We proceed to treat order by order in \mathbf{A} through Subsections 4.1, 4.2 and 4.3. There, we suppose that all functions are evaluated precisely at the bifurcation point $\mu = \mu^*$. Subsection 4.4 deals with the unfolding of the bifurcation. That is, the computation of the leading-order coefficient of $|\mu - \mu^*|$ in the normal form.

Suppose that, at the bifurcation point $\mu = \mu^*$ the ground state \mathbf{P} fulfills the conditions stated in Theorem 1. We proceed to build the normal form using ansatz (7). In particular, we shall prove that $\mathbf{A} = (A_{-\ell}, A_{-\ell+1}, \dots, A_{\ell-1}, A_\ell)^\top$ solves an equation of the form

$$\partial_t \mathbf{A} = \sum_{m_1=-\ell}^{\ell} \mathbf{h}_{m_1}^{[1]}(A_{m_1}) + \sum_{-\ell \leq m_1, m_2 \leq \ell} \mathbf{h}_{m_1, m_2}^{[2]}(A_{m_1}, A_{m_2}) + \dots, \quad (24)$$

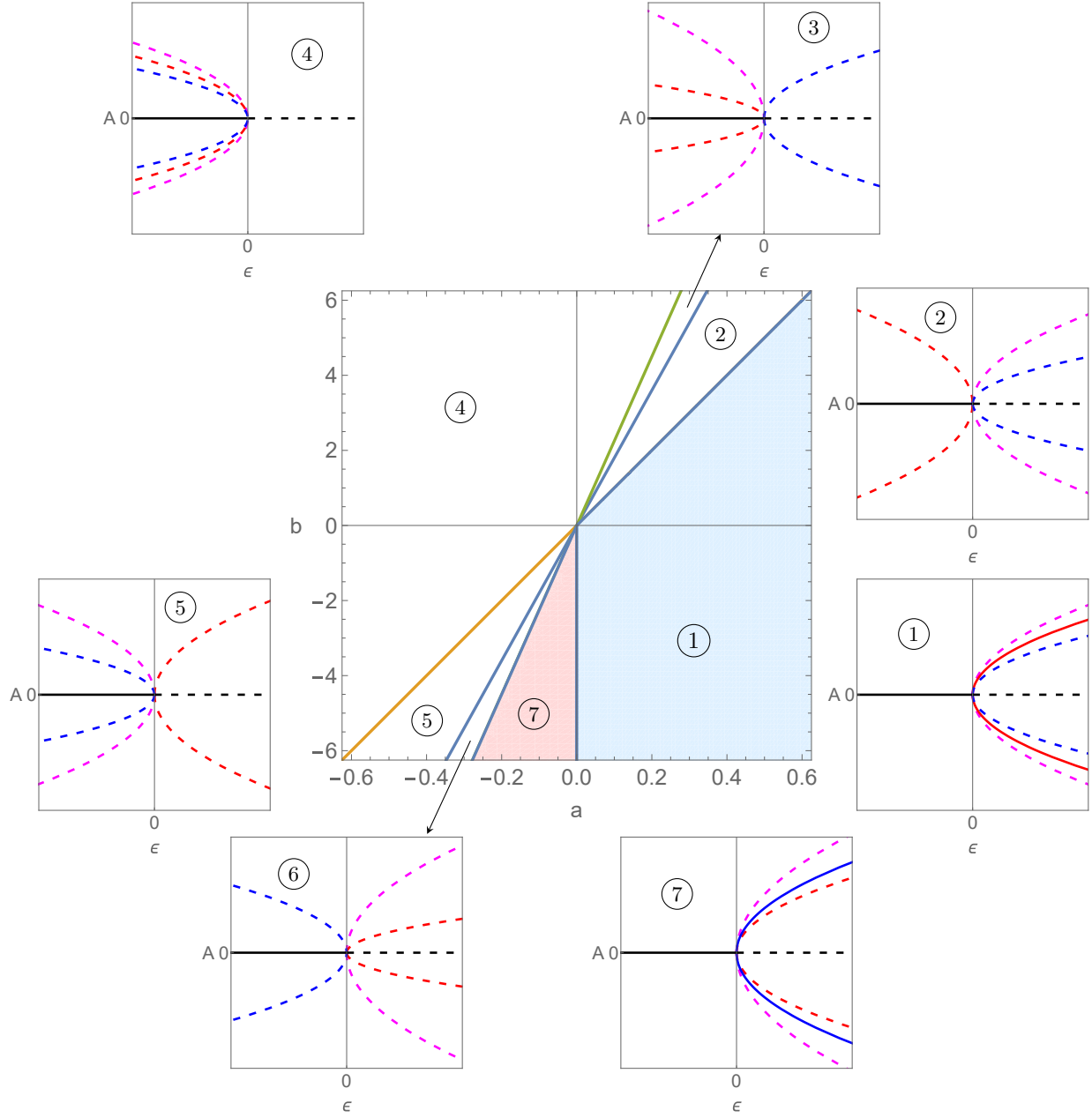


Figure 3: Partial bifurcation diagram for the pitchfork bifurcation of the normal form (22) that arises when $\ell = 3$. Magenta, red, and blue curves represent the steady states with symmetries $O(2)^-$, \mathbf{O} , and D_6^d , respectively. Moreover, dashed (resp. continuous) lines represent unstable (resp. stable) steady states. In the $a - b$ bifurcation diagram, the straight lines are given by: $18a - b = 0$, $10a - b = 0$ and $45a - 2b = 0$.

where each function $\mathbf{h}_{m_1, \dots, m_p}^{[p]}(A_{m_1}, \dots, A_{m_p})$ corresponds to a linear function in $\prod_{j=1}^p A_{m_j}$. To find these functions, we use the ansatz

$$\begin{pmatrix} \mathbf{U} \\ \mathbf{u} \end{pmatrix} = \mathbf{P} + \sum_{q_1=-\ell}^{\ell} \mathbf{W}_{q_1}^{[1]}(A_{q_1}) + \sum_{-\ell \leq q_1, q_2 \leq \ell} \mathbf{W}_{q_1, q_2}^{[2]}(A_{q_1}, A_{q_2}) + \dots,$$

where we need to find the vector functions $\mathbf{W}_{q_1}^{[1]}, \mathbf{W}_{q_1, q_2}^{[2]}, \dots$ such that \mathbf{A} solves an equation of the form (24). We proceed order by order.

4.1 Order 1

At this order, (1) becomes

$$\sum_{q_1=-\ell}^{\ell} \partial_{A_{q_1}} \mathbf{W}_{q_1}^{[1]} \sum_{m_1=-\ell}^{\ell} h_{m_1, q_1}^{[1]} = \sum_{q_1=-\ell}^{\ell} (J_{\mathbf{u}} \mathbf{f}(\mathbf{P}) + \mathbb{D} \nabla^2) \mathbf{W}_{q_1}^{[1]}, \quad (25)$$

where q_1 in the sub-script of $h_{m_1, q_1}^{[1]}$ indicates the component of $\mathbf{h}_{m_1}^{[1]}$. Therefore, if we choose $h_{m_1, q_1}^{[1]} \equiv 0$ for every $-\ell \leq m_1, q_1 \leq \ell$, then (25) becomes:

$$\sum_{q_1=-\ell}^{\ell} (J_{\mathbf{u}} \mathbf{f}(\mathbf{P}) + \mathbb{D} \nabla^2) \mathbf{W}_{q_1}^{[1]} = \mathbf{0}. \quad (26)$$

Here, note that the sum on the left-hand side is taken over all the amplitudes, which multiply orthogonal functions. Therefore, we must set each component of the sum to zero independently. Thus, for each q_1 , we must find $\mathbf{W}_{q_1}^{[1]} = (\mathbf{U}(r, \theta, \phi), \mathbf{u}(\theta, \phi))^{\top}$ such that

$$(J_{\mathbf{u}} \mathbf{f}(\mathbf{P}) + \mathbb{D} \nabla^2) \begin{pmatrix} \mathbf{U} \\ \mathbf{u} \end{pmatrix} = \mathbf{0}.$$

Now, note that the first n equations can be written as $-B \mathbf{U} + \mathbb{D}_U \nabla_{\Omega}^2 \mathbf{U} = \mathbf{0}$, from where we can choose the following non-zero solution $\mathbf{U} = i_{\ell}(\omega r) P_{\ell}^m(\cos(\theta)) e^{im\phi} \hat{\boldsymbol{\varphi}}$, where $\hat{\boldsymbol{\varphi}} \in \mathbb{R}^n \setminus \{\mathbf{0}\}$ is a constant vector, and $i_{\ell}(\omega r) = \text{diag}(i_{\ell}(\omega_1 r), \dots, i_{\ell}(\omega_n r))$, with i_{ℓ} being a modified spherical Bessel function of the first kind. Therefore, if we take $\mathbf{u} = P_{\ell}^m(\cos(\theta)) e^{im\phi} \boldsymbol{\varphi}$, the boundary conditions imply that $\hat{\boldsymbol{\varphi}} = S_{\ell} \boldsymbol{\varphi}$. Thus, the last n equations of (26) become $\det(\mathbb{B}_{\ell}) = 0$, which implies

$$\left(K(i_{\ell}(\omega R) S_{\ell} - I) + J_{\mathbf{u}} \mathbf{g}(\mathbf{u}^*) - \frac{\ell(\ell+1)}{R^2} \mathbb{D}_u \right) \boldsymbol{\varphi} = \mathbf{0}.$$

This equation has a one-parameter family of nontrivial solutions as, by assumption,

$$\det \left(K(i_{\ell}(\omega R) S_{\ell} - I) + J_{\mathbf{u}} \mathbf{g}(\mathbf{u}^*) - \frac{\ell(\ell+1)}{R^2} \mathbb{D}_u \right) = 0.$$

We can choose $\boldsymbol{\varphi}$ to be any non-zero vector in the kernel. With this, we define the non-zero vector

$$\mathbf{W}_{q_1}^{[1]} = \begin{pmatrix} \mathbf{W}_{q_1, 1}^{[1]} \\ \mathbf{W}_{q_1, 2}^{[1]} \end{pmatrix} = A_{q_1} \begin{pmatrix} i_{\ell}(\omega r) \hat{\boldsymbol{\varphi}} \\ \boldsymbol{\varphi} \end{pmatrix} P_{\ell}^{q_1}(\cos(\theta)) e^{iq_1\phi},$$

where

$$\left(K(i_{\ell}(\omega R) S_{\ell} - I) + J_{\mathbf{u}} \mathbf{g}(\mathbf{u}^*) - \frac{\ell(\ell+1)}{R^2} \mathbb{D}_u \right) \boldsymbol{\varphi} = \mathbf{0}, \quad \text{and} \quad \hat{\boldsymbol{\varphi}} = S_{\ell} \boldsymbol{\varphi}.$$

4.2 Order 2

At this order, (1) becomes

$$\begin{aligned} \sum_{b=-\ell}^{\ell} \partial_{A_b} \mathbf{W}_b^{[1]} \sum_{-\ell \leq q_1, q_2 \leq \ell} h_{q_1, q_2, b}^{[2]} &= \sum_{-\ell \leq q_1, q_2 \leq \ell} (J_{\mathbf{u}} \mathbf{f}(\mathbf{P}) + \mathbb{D} \nabla^2) \mathbf{W}_{q_1, q_2}^{[2]} \\ &+ \sum_{-\ell \leq q_1, q_2 \leq \ell} \left(\mathbf{G}_2 \left(\mathbf{W}_{q_1, 2}^{[1]}, \mathbf{W}_{q_2, 2}^{[1]} \right) \right), \end{aligned} \quad (27)$$

which is equivalent to

$$\begin{aligned} \sum_{-\ell \leq q_1, q_2 \leq \ell} (J_{\mathbf{u}} \mathbf{f}(\mathbf{P}) + \mathbb{D} \nabla^2) \mathbf{W}_{q_1, q_2}^{[2]} &= \sum_{b=-\ell}^{\ell} \partial_{A_b} \mathbf{W}_b^{[1]} \sum_{-\ell \leq q_1, q_2 \leq \ell} h_{q_1, q_2, b}^{[2]} \\ &- \sum_{-\ell \leq q_1, q_2 \leq \ell} A_{q_1} A_{q_2} P_{\ell}^{q_1}(\cos(\theta)) P_{\ell}^{q_2}(\cos(\theta)) e^{i(q_1+q_2)\phi} \left(\mathbf{G}_2(\boldsymbol{\varphi}, \boldsymbol{\varphi}) \right). \end{aligned}$$

Here, the subscript b on h refers to the coefficient of the corresponding quadratic term $A_{q_1} A_{q_2}$.

Before continuing, we need to choose an inner product, to establish solvability conditions using the Fredholm alternative. We make the following natural choice: suppose for $\mathbf{a}_1, \mathbf{a}_2, \mathbf{b}_1, \mathbf{b}_2 \in \mathbb{C}^n$, $f_1, g_1 \in \mathcal{L}^2(\Omega; \mathbb{R})$, and $f_2, g_2 \in \mathcal{L}^2(\Gamma; \mathbb{R})$, then we define

$$\begin{aligned} \left\langle \begin{pmatrix} f_1 \mathbf{a}_1 \\ f_2 \mathbf{a}_2 \end{pmatrix}, \begin{pmatrix} g_1 \mathbf{b}_1 \\ g_2 \mathbf{b}_2 \end{pmatrix} \right\rangle &:= \frac{1}{2\pi} \left(\iiint_{\Omega} f_1(x, y, z) \mathbf{a}_1 \cdot \overline{g_1(x, y, z) \mathbf{b}_1} d\Omega \right. \\ &+ R^2 \iint_{\Gamma} f_2(x, y, z) \mathbf{a}_2 \cdot \overline{g_2(x, y, z) \mathbf{b}_2} d\Gamma \left. \right) \\ &= \frac{1}{2\pi} \left(\int_0^R \int_0^{2\pi} \int_0^{\pi} f_1(r, \theta, \phi) \mathbf{a}_1 \cdot \overline{g_1(r, \theta, \phi) \mathbf{b}_1} r^2 \sin(\theta) d\theta d\phi dr \right. \\ &+ R^2 \int_0^{2\pi} \int_0^{\pi} f_2(\theta, \phi) \mathbf{a}_2 \cdot \overline{g_2(\theta, \phi) \mathbf{b}_2} \sin(\theta) d\theta d\phi \left. \right), \end{aligned} \quad (28)$$

where \cdot denotes the usual scalar product of n -component vectors.

Now, we want to expand $P_{\ell}^{q_1}(\cos(\theta)) P_{\ell}^{q_2}(\cos(\theta))$ in terms of the family of functions $\{P_p^{q_1+q_2}(\cos(\theta))\}_{p=|q_1+q_2|}^{\infty}$. To do this, consider the following result.

Lemma 2. *For every $-\ell \leq q_1, q_2 \leq \ell$, the function $P_{\ell}^{q_1}(x) P_{\ell}^{q_2}(x)$ can be written as a linear combination of $\{P_p^{q_1+q_2}(x)\}_{p=|q_1+q_2|}^{2\ell}$.*

Proof. As the associated Legendre polynomials fulfill $P_{\ell}^{-m}(x) = (-1)^m P_{\ell}^m(x)$, then we assume, without loss of generality, that $q_1, q_2 > 0$. By definition, for $\ell \in \mathbb{Z}$ with $0 \leq m \leq \ell$, $P_{\ell}^m(x) = \mathcal{N}_{\ell, m} (1-x^2)^{m/2} \frac{d^{\ell+m}}{dx^{\ell+m}} (x^2-1)^{\ell}$, where $\mathcal{N}_{\ell, m} \in \mathbb{R}$ is a constant that normalizes the associated Legendre polynomial. Note that

$$\frac{P_{\ell}^{q_1}(x) P_{\ell}^{q_2}(x)}{(1-x^2)^{(q_1+q_2)/2}} = \mathcal{N}_{\ell, q_1} \mathcal{N}_{\ell, q_2} \frac{d^{\ell+q_1}}{dx^{\ell+q_1}} (x^2-1)^{\ell} \frac{d^{\ell+q_2}}{dx^{\ell+q_2}} (x^2-1)^{\ell},$$

is a polynomial of degree $2\ell - (q_1 + q_2)$, and

$$\frac{P_p^{q_1+q_2}(x)}{(1-x^2)^{(q_1+q_2)/2}} = \mathcal{N}_{p, q_1+q_2} \frac{d^{p+q_1+q_2}}{dx^{p+q_1+q_2}} (x^2-1)^p, \quad (29)$$

is a polynomial of degree $p - (q_1 + q_2)$, for $p \geq q_1 + q_2$. Moreover, note that $P_p^{q_1+q_2} \equiv 0$ when $|q_1 + q_2| > p$.

Hence, this implies that the family of polynomials $\left\{ \frac{P_p^{q_1+q_2}(x)}{(1-x^2)^{(q_1+q_2)/2}} \right\}_{p=|q_1+q_2|}^{2\ell}$ forms a basis of the space of polynomials of degree $2\ell - (q_1 + q_2)$. Thus, $P_{\ell}^{q_1}(x) P_{\ell}^{q_2}(x)$ can be expanded as a linear combination of $\{P_p^{q_1+q_2}(x)\}_{p=|q_1+q_2|}^{2\ell}$, which concludes the proof. \square

Now, thanks to Lemma 2 and the inner product (28), we have

$$P_\ell^{q_1}(\cos(\theta)) P_\ell^{q_2}(\cos(\theta)) = \sum_{p=|q_1+q_2|}^{2\ell} d_{p,q_1,q_2}^{[2]} P_p^{q_1+q_2}(\cos(\theta)),$$

where

$$\begin{aligned} d_{p,q_1,q_2}^{[2]} &= \int_0^\pi P_\ell^{q_1}(\cos(\theta)) P_\ell^{q_2}(\cos(\theta)) P_p^{q_1+q_2}(\cos(\theta)) \sin(\theta) d\theta \\ &= \int_{-1}^1 P_\ell^{q_1}(x) P_\ell^{q_2}(x) P_p^{q_1+q_2}(x) dx, \end{aligned}$$

for every integer $|q_1 + q_2| \leq p \leq 2\ell$. Owing to the parity of the associated Legendre polynomials, it follows that $d_{p,q_1,q_2}^{[2]} = 0$, for every odd p .

With this, equation (27) becomes

$$\begin{aligned} \sum_{-\ell \leq q_1, q_2 \leq \ell} (J_{\mathbf{u}} \mathbf{f}(\mathbf{P}) + \mathbb{D} \nabla^2) \mathbf{W}_{q_1, q_2}^{[2]} &= \sum_{b=-\ell}^{\ell} \partial_{A_b} \mathbf{W}_b^{[1]} \sum_{-\ell \leq q_1, q_2 \leq \ell} h_{q_1, q_2, b}^{[2]} \\ &\quad - \sum_{-\ell \leq q_1, q_2 \leq \ell} A_{q_1} A_{q_2} \sum_{p=|q_1+q_2|}^{2\ell} d_{p,q_1,q_2}^{[2]} P_p^{q_1+q_2}(\cos(\theta)) e^{i(q_1+q_2)\phi} \begin{pmatrix} \mathbf{0}_n \\ \mathbf{G}_2(\boldsymbol{\varphi}, \boldsymbol{\varphi}) \end{pmatrix}. \end{aligned} \quad (30)$$

Here, there might be secular terms if ℓ is even [39], in which case there is a solvability condition that can be used to determine $\mathbf{h}_{q_1, q_2}^{[2]}$. To find it, we can use the Fredholm alternative with the vector functions $\boldsymbol{\psi}_m^*$, for $m \in \mathbb{Z}$, that span

$\ker \left((J_{\mathbf{u}} \mathbf{f}(\mathbf{P}) + \mathbb{D} \nabla^2)^* \right)$. We have the following result.

Lemma 3. *With the inner product defined by (28), we have that*

$$(J_{\mathbf{u}} \mathbf{f}(\mathbf{P}) + \mathbb{D} \nabla^2)^* = \begin{pmatrix} -B + \mathbb{D}_U \nabla_\Omega^2 & \mathbf{0}_{n \times n} \\ K I|_\Gamma & -K + J_{\mathbf{u}} \mathbf{g}(\mathbf{u}^*)^\top + \mathbb{D}_u^\top \nabla_\Gamma^2 \end{pmatrix}.$$

Proof. By the definition of the adjoint matrix

$$\begin{aligned} \left\langle (J_{\mathbf{u}} \mathbf{f}(\mathbf{P}) + \mathbb{D} \nabla^2)^* \begin{pmatrix} \hat{\mathbf{U}} \\ \hat{\mathbf{u}} \end{pmatrix}, \begin{pmatrix} \mathbf{U} \\ \mathbf{u} \end{pmatrix} \right\rangle &= \frac{1}{2\pi} \left(\iiint_\Omega (-B \hat{\mathbf{U}} \cdot \bar{\mathbf{U}} + \mathbb{D}_U \nabla_\Omega^2 \hat{\mathbf{U}} \cdot \bar{\mathbf{U}}) d\Omega \right. \\ &\quad \left. + R^2 \iint_\Gamma (K \hat{\mathbf{U}}|_\Gamma \cdot \bar{\mathbf{u}} - K \hat{\mathbf{u}} \cdot \bar{\mathbf{u}} + J_{\mathbf{u}} \mathbf{g}(\mathbf{u}^*)^\top \hat{\mathbf{u}} \cdot \bar{\mathbf{u}} + \mathbb{D}_u^\top \nabla_\Gamma^2 \hat{\mathbf{u}} \cdot \bar{\mathbf{u}}) d\Gamma \right), \end{aligned}$$

and

$$\begin{aligned} \left\langle \begin{pmatrix} \hat{\mathbf{U}} \\ \hat{\mathbf{u}} \end{pmatrix}, (J_{\mathbf{u}} \mathbf{f}(\mathbf{P}) + \mathbb{D} \nabla^2) \begin{pmatrix} \mathbf{U} \\ \mathbf{u} \end{pmatrix} \right\rangle &= \frac{1}{2\pi} \left(\iiint_\Omega (-B \bar{\mathbf{U}} \cdot \hat{\mathbf{U}} + \mathbb{D}_U \nabla_\Omega^2 \bar{\mathbf{U}} \cdot \hat{\mathbf{U}}) d\Omega \right. \\ &\quad \left. + R^2 \iint_\Gamma (K \bar{\mathbf{U}}|_\Gamma \cdot \hat{\mathbf{u}} - K \bar{\mathbf{u}} \cdot \hat{\mathbf{u}} + J_{\mathbf{u}} \mathbf{g}(\mathbf{u}^*) \bar{\mathbf{u}} \cdot \hat{\mathbf{u}} + \mathbb{D}_u \nabla_\Gamma^2 \bar{\mathbf{u}} \cdot \hat{\mathbf{u}}) d\Gamma \right). \end{aligned}$$

Therefore,

$$\begin{aligned} \left\langle (J_{\mathbf{u}} \mathbf{f}(\mathbf{P}) + \mathbb{D} \nabla^2)^* \begin{pmatrix} \hat{\mathbf{U}} \\ \hat{\mathbf{u}} \end{pmatrix}, \begin{pmatrix} \mathbf{U} \\ \mathbf{u} \end{pmatrix} \right\rangle &- \left\langle \begin{pmatrix} \hat{\mathbf{U}} \\ \hat{\mathbf{u}} \end{pmatrix}, (J_{\mathbf{u}} \mathbf{f}(\mathbf{P}) + \mathbb{D} \nabla^2) \begin{pmatrix} \mathbf{U} \\ \mathbf{u} \end{pmatrix} \right\rangle \\ &= \frac{1}{2\pi} \left(\iint_\Gamma \left(\mathbb{D}_U \frac{d\hat{\mathbf{U}}}{d\nu} \Big|_\Gamma \cdot \bar{\mathbf{U}}|_\Gamma - \mathbb{D}_U \frac{d\bar{\mathbf{U}}}{d\nu} \Big|_\Gamma \cdot \hat{\mathbf{U}}|_\Gamma \right) d\Omega \right. \\ &\quad \left. + R^2 \iint_\Gamma (K \hat{\mathbf{U}}|_\Gamma \cdot \bar{\mathbf{u}} - K \bar{\mathbf{U}}|_\Gamma \cdot \hat{\mathbf{u}}) d\Gamma \right) = 0, \end{aligned}$$

which proves the result. \square

Now, for $m \in \mathbb{Z}$, ψ_m^* solves the following equation $(J_{\mathbf{u}} \mathbf{f}(\mathbf{P}) + \mathbb{D} \nabla^2)^* \psi_m^* = \mathbf{0}$. Furthermore, by Lemma 3, we know that φ_m^* has the following form

$$\psi_m^* = \begin{pmatrix} i_\ell(\omega r) \hat{\psi} \\ \psi \end{pmatrix} P_\ell^m(\cos(\theta)) e^{im\phi}, \text{ for each integer } -\ell \leq m \leq \ell, \text{ where}$$

$$\left(K(i_\ell(\omega R) S_\ell - I) + J_{\mathbf{u}} \mathbf{g}(\mathbf{u}^*)^\top - \frac{\ell(\ell+1)}{R^2} \mathbb{D}_{\mathbf{u}}^\top \right) \psi = \mathbf{0}, \quad \text{and} \quad \hat{\psi} = S_\ell \psi.$$

Therefore, if we split equation (27) according to the amplitudes, and apply the inner product with respect to a single function ψ_m^* , we get the following expression

$$\begin{aligned} \left\langle (J_{\mathbf{u}} \mathbf{f}(\mathbf{P}) + \mathbb{D} \nabla^2) \mathbf{W}_{q_1, q_2}^{[2]}, \psi_m^* \right\rangle &= \left\langle \begin{pmatrix} i_\ell(\omega r) \hat{\varphi} \\ \varphi \end{pmatrix} P_\ell^m(\cos(\theta)) e^{im\phi} h_{q_1, q_2, m}^{[2]}, \psi_m^* \right\rangle \\ &\quad - A_{q_1} A_{q_2} \left\langle \sum_{p=|q_1+q_2|}^{2\ell} d_{p, q_1, q_2}^{[2]} P_p^{q_1+q_2}(\cos(\theta)) e^{i(q_1+q_2)\phi} \begin{pmatrix} \mathbf{0}_n \\ \mathbf{G}_2(\varphi, \varphi) \end{pmatrix}, \psi_m^* \right\rangle, \end{aligned}$$

which can be expanded as

$$\begin{aligned} &\left\langle (J_{\mathbf{u}} \mathbf{f}(\mathbf{P}) + \mathbb{D} \nabla^2) \mathbf{W}_{q_1, q_2}^{[2]}, \psi_m^* \right\rangle \\ &= \left(\int_0^R i_\ell(\omega r) S_\ell \varphi \cdot i_\ell(\omega r) S_\ell \psi r^2 dr + R^2 \varphi \cdot \psi \right) - A_{q_1} A_{q_2} R^2 \delta_{m, q_1+q_2} \times \\ &\quad \mathbf{G}_2(\varphi, \varphi) \cdot \psi \sum_{p=|q_1+q_2|}^{2\ell} d_{p, q_1, q_2}^{[2]} \int_0^\pi P_p^{q_1+q_2}(\cos(\theta)) P_\ell^m(\cos(\theta)) \sin(\theta) d\theta. \end{aligned}$$

Therefore, when we set this expression to zero, we see that $h_{q_1, q_2, m}^{[2]} = C_{q_1, q_2, m}^{[2]} A_{q_1} A_{q_2}$, where

$$\begin{aligned} C_{q_1, q_2, m}^{[2]} &= \frac{R^2}{I_\ell} \delta_{m, q_1+q_2} d_{\ell, q_1, q_2}^{[2]} \mathbf{G}_2(\varphi, \varphi) \cdot \psi, \quad \text{with} \\ I_\ell &= \int_0^R i_\ell(\omega r) S_\ell \varphi \cdot i_\ell(\omega r) S_\ell \psi r^2 dr + R^2 \varphi \cdot \psi. \end{aligned} \tag{31}$$

These coefficients are sufficient to classify generic transcritical bifurcations that occur when ℓ is even. However for odd ℓ or if the quadratic coefficient vanishes for even ℓ , we need to go further to compute cubic terms.

To simplify the computation of cubic terms, we assume that $h_{q_1, q_2, m}^{[2]} = 0$. Under this assumption, the solution to (30) that is orthogonal to $\ker(J_{\mathbf{u}} \mathbf{f}(\mathbf{P}) + \mathbb{D} \nabla^2)$ is given by

$$\mathbf{W}_{q_1, q_2}^{[2]} = \begin{pmatrix} \mathbf{W}_{q_1, q_2, 1}^{[2]} \\ \mathbf{W}_{q_1, q_2, 2}^{[2]} \end{pmatrix} = A_{q_1} A_{q_2} \left(\sum_{p=|q_1+q_2|}^{2\ell} \begin{pmatrix} i_p(\omega r) \mathbf{U}_{p, q_1, q_2}^{[2]} \\ \mathbf{u}_{p, q_1, q_2}^{[2]} \end{pmatrix} P_p^{q_1+q_2}(\cos(\theta)) e^{i(q_1+q_2)\phi} \right),$$

where $\mathbb{B}_p \mathbf{u}_{p, q_1, q_2}^{[2]} = -d_{p, q_1, q_2}^{[2]} \mathbf{G}_2(\varphi, \varphi)$, and $\mathbf{U}_{p, q_1, q_2}^{[2]} = S_p \mathbf{u}_{p, q_1, q_2}^{[2]}$, for each integer $|q_1 + q_2| \leq p \leq 2\ell$.

Note that these systems of equations have a solution for every $|q_1 + q_2| \leq p \leq 2\ell$ since $d_{p, q_1, q_2}^{[2]} = 0$ for every odd p and, if ℓ is odd, we stated in Theorem 1 that \mathbb{B}_p is invertible when p is even. On the other hand, if ℓ is even, then although \mathbb{B}_ℓ is non-invertible, the right-hand side belongs to its image when $p = \ell$.

With this, we are ready to proceed to the next order.

4.3 Order 3

At this order, equation (1) becomes

$$\sum_{b=-\ell}^{\ell} \partial_{A_b} \mathbf{W}_b^{[1]} \sum_{-\ell \leq m_1, m_2, m_3 \leq \ell} h_{m_1, m_2, m_3, b}^{[3]}$$

$$\begin{aligned}
&= \sum_{-\ell \leq q_1, q_2, q_3 \leq \ell} (J_{\mathbf{u}} \mathbf{f}(\mathbf{P}) + \mathbb{D} \nabla^2) \mathbf{W}_{q_1, q_2, q_3}^{[3]} + 2 \sum_{-\ell \leq q_1, q_2, q_3 \leq \ell} \left(\mathbf{G}_2 \left(\mathbf{W}_{q_1, q_2, 2}^{[2]}, \mathbf{W}_{q_3, 2}^{[1]} \right) \right) \\
&\quad + \sum_{-\ell \leq q_1, q_2, q_3 \leq \ell} \left(\mathbf{G}_3 \left(\mathbf{W}_{q_1, 2}^{[1]}, \mathbf{W}_{q_2, 2}^{[1]}, \mathbf{W}_{q_3, 2}^{[1]} \right) \right).
\end{aligned}$$

This entails

$$\begin{aligned}
&\sum_{-\ell \leq q_1, q_2, q_3 \leq \ell} (J_{\mathbf{u}} \mathbf{f}(\mathbf{P}) + \mathbb{D} \nabla^2) \mathbf{W}_{q_1, q_2, q_3}^{[3]} = \sum_{b=-\ell}^{\ell} \partial_{A_b} \mathbf{W}_b^{[1]} \sum_{-\ell \leq m_1, m_2, m_3 \leq \ell} h_{m_1, m_2, m_3, b}^{[3]} \\
&\quad - 2 \sum_{-\ell \leq q_1, q_2, q_3 \leq \ell} A_{q_1} A_{q_2} A_{q_3} P_{\ell}^{q_3}(\cos(\theta)) e^{iq_3 \phi} \sum_{p=|q_1+q_2|}^{2\ell} P_p^{q_1+q_2}(\cos(\theta)) e^{i(q_1+q_2)\phi} \times \\
&\quad \left(\mathbf{G}_2 \left(\mathbf{u}_{p, q_1, q_2}^{[2]}, \boldsymbol{\varphi} \right) \right) - \sum_{-\ell \leq q_1, q_2, q_3 \leq \ell} A_{q_1} A_{q_2} A_{q_3} P_{\ell}^{q_1}(\cos(\theta)) \times \\
&\quad P_{\ell}^{q_2}(\cos(\theta)) P_{\ell}^{q_3}(\cos(\theta)) e^{i(q_1+q_2+q_3)\phi} \left(\mathbf{G}_3 \left(\boldsymbol{\varphi}, \boldsymbol{\varphi}, \boldsymbol{\varphi} \right) \right).
\end{aligned}$$

Therefore, by splitting this equation according to the amplitudes we see that, for every $-\ell \leq q_1, q_2, q_3 \leq \ell$,

$$\begin{aligned}
(J_{\mathbf{u}} \mathbf{f}(\mathbf{P}) + \mathbb{D} \nabla^2) \mathbf{W}_{q_1, q_2, q_3}^{[3]} &= \sum_{b=-\ell}^{\ell} \begin{pmatrix} i_{\ell}(\boldsymbol{\omega} r) \hat{\boldsymbol{\varphi}} \\ \boldsymbol{\varphi} \end{pmatrix} P_{\ell}^b(\cos(\theta)) e^{ib\phi} h_{q_1, q_2, q_3, b}^{[3]} \\
&\quad - 2 P_{\ell}^{q_3}(\cos(\theta)) \sum_{p=|q_1+q_2|}^{2\ell} P_p^{q_1+q_2}(\cos(\theta)) e^{i(q_1+q_2+q_3)\phi} \left(\mathbf{G}_2 \left(\mathbf{u}_{p, q_1, q_2}^{[2]}, \boldsymbol{\varphi} \right) \right) \\
&\quad - P_{\ell}^{q_1}(\cos(\theta)) P_{\ell}^{q_2}(\cos(\theta)) P_{\ell}^{q_3}(\cos(\theta)) e^{i(q_1+q_2+q_3)\phi} \left(\mathbf{G}_3 \left(\boldsymbol{\varphi}, \boldsymbol{\varphi}, \boldsymbol{\varphi} \right) \right). \quad (32)
\end{aligned}$$

Thus, when we apply the inner product with $\boldsymbol{\psi}_m^*$ in (32), we get the following expression

$$\begin{aligned}
&\left\langle (J_{\mathbf{u}} \mathbf{f}(\mathbf{P}) + \mathbb{D} \nabla^2) \mathbf{W}_{q_1, q_2, q_3}^{[3]}, \boldsymbol{\psi}_m^* \right\rangle \\
&= \sum_{b=-\ell}^{\ell} \left\langle \begin{pmatrix} i_{\ell}(\boldsymbol{\omega} r) \hat{\boldsymbol{\varphi}} \\ \boldsymbol{\varphi} \end{pmatrix} P_{\ell}^b(\cos(\theta)) e^{ib\phi} h_{q_1, q_2, q_3, b}^{[3]}, \boldsymbol{\psi}_m^* \right\rangle \\
&\quad - 2 \left\langle P_{\ell}^{q_3}(\cos(\theta)) \sum_{p=|q_1+q_2|}^{2\ell} P_p^{q_1+q_2}(\cos(\theta)) e^{i(q_1+q_2+q_3)\phi} \left(\mathbf{G}_2 \left(\mathbf{u}_{p, q_1, q_2}^{[2]}, \boldsymbol{\varphi} \right) \right), \boldsymbol{\psi}_m^* \right\rangle \\
&\quad - \left\langle P_{\ell}^{q_1}(\cos(\theta)) P_{\ell}^{q_2}(\cos(\theta)) P_{\ell}^{q_3}(\cos(\theta)) e^{i(q_1+q_2+q_3)\phi} \left(\mathbf{G}_3 \left(\boldsymbol{\varphi}, \boldsymbol{\varphi}, \boldsymbol{\varphi} \right) \right), \boldsymbol{\psi}_m^* \right\rangle,
\end{aligned}$$

which can be expanded as

$$\begin{aligned}
&\left\langle (J_{\mathbf{u}} \mathbf{f}(\mathbf{P}) + \mathbb{D} \nabla^2) \mathbf{W}_{q_1, q_2, q_3}^{[3]}, \boldsymbol{\psi}_m^* \right\rangle \\
&= \left(\int_0^R i_{\ell}(\boldsymbol{\omega} r) S_{\ell} \boldsymbol{\varphi} \cdot i_{\ell}(\boldsymbol{\omega} r) S_{\ell} \boldsymbol{\psi} r^2 dr + R^2 \boldsymbol{\varphi} \cdot \boldsymbol{\psi} \right) h_{q_1, q_2, q_3, m}^{[3]} - 2 \delta_{m, q_1+q_2+q_3} R^2 \times \\
&\quad \sum_{p=|q_1+q_2|}^{2\ell} \mathbf{G}_2 \left(\mathbf{u}_{p, q_1, q_2}^{[2]}, \boldsymbol{\varphi} \right) \cdot \boldsymbol{\psi} \int_0^{\pi} P_{\ell}^{q_3}(\cos(\theta)) P_p^{q_1+q_2}(\cos(\theta)) P_{\ell}^m(\cos(\theta)) \sin(\theta) d\theta \\
&\quad - \delta_{m, q_1+q_2+q_3} R^2 \mathbf{G}_3 \left(\boldsymbol{\varphi}, \boldsymbol{\varphi}, \boldsymbol{\varphi} \right) \cdot \boldsymbol{\psi} \times
\end{aligned}$$

$$\int_0^\pi P_\ell^{q_1}(\cos(\theta)) P_\ell^{q_2}(\cos(\theta)) P_\ell^{q_3}(\cos(\theta)) P_\ell^m(\cos(\theta)) \sin(\theta) d\theta.$$

Finally, the solvability condition comes from equating this expression to zero, which leads us to conclude that $h_{q_1, q_2, q_3, m}^{[3]}(\mathbf{A}) = C_{q_1, q_2, q_3, m}^{[3]} A_{q_1} A_{q_2} A_{q_3}$, where

$$C_{q_1, q_2, q_3, m}^{[3]} = \frac{R^2}{I_\ell} \delta_{m, q_1 + q_2 + q_3} \left(2 \sum_{p=|q_1+q_2|}^{2\ell} \mathbf{G}_2 \left(\mathbf{u}_{p, q_1, q_2}^{[2]}, \boldsymbol{\varphi} \right) \cdot \boldsymbol{\psi} \int_{-1}^1 P_\ell^{q_3}(x) P_p^{q_1+q_2}(x) \times \right. \\ \left. P_\ell^m(x) dx + \mathbf{G}_3(\boldsymbol{\varphi}, \boldsymbol{\varphi}, \boldsymbol{\varphi}) \cdot \boldsymbol{\psi} \int_{-1}^1 P_\ell^{q_1}(x) P_\ell^{q_2}(x) P_\ell^{q_3}(x) P_\ell^m(x) dx \right), \quad (33)$$

4.4 Unfolding

The calculation so far has been performed under the assumption that we are precisely at the bifurcation point $\mu = \mu^*$. Now, we recall that, for the first part of the proof, we set To study what happens for small $\mu - \mu^*$, we now want A to solve a differential equation of the following form

$$\partial_t \mathbf{A} = \sum_{m_1=-\ell}^{\ell} \mathbf{h}_{m_1}^{[1,1]}(A_{m_1}, \mu) + \sum_{m_1=-\ell}^{\ell} \mathbf{h}_{m_1}^{[1,0]}(A_{m_1}, \mu) + \sum_{-\ell \leq m_1 \leq m_2 \leq \ell} \mathbf{h}_{m_1, m_2}^{[2,0]}(A_{m_1}, A_{m_2}, \mu) + \dots,$$

where the superscripts stand for the degree of each polynomial in \mathbf{A} and $\mu - \mu^*$, respectively. In particular, note that for each $p = 1, 2, 3$, $\mathbf{h}_{m_1, m_2, \dots}^{[p,0]}(A_{m_1}, A_{m_2}, \dots, \mu) = \mathbf{h}_{m_1, m_2, \dots}^{[p]}(A_{m_1}, A_{m_2}, \dots)$, which corresponds to one of the terms we calculated in the preceding subsections. We extend this by considering a change of variables with the following form

$$\begin{pmatrix} \mathbf{U} \\ \mathbf{u} \end{pmatrix} = \mathbf{P} + \sum_{q_1=-\ell}^{\ell} \mathbf{W}_{q_1}^{[1,1]}(A_{q_1}, \mu) + \sum_{q_1=-\ell}^{\ell} \mathbf{W}_{q_1}^{[1,0]}(A_{q_1}, \mu) + \sum_{-\ell \leq q_1, q_2 \leq \ell} \mathbf{W}_{q_1, q_2}^{[2,0]}(A_{q_1}, A_{q_2}, \mu) + \dots,$$

where we only consider the leading-order unfolding term (see e.g. [41], and the terms $\mathbf{W}_{q_1, q_2, \dots}^{[p,0]}(A_{q_1}, A_{q_2}, \dots, \mu)$ for $p = 1, 2, 3$, were already found. Thus we only need to find $\mathbf{h}_{m_1}^{[1,1]}(A_{m_1}, \mu)$, which we do by considering only the terms in the Taylor expansion of (1) that have a product between μ and one amplitude A_p , for $-\ell \leq p \leq \ell$ and μ . Carefully summing such terms leads to the following expression

$$\sum_{b=-\ell}^{\ell} \partial_{A_b} \mathbf{W}_b^{[1,0]} \sum_{m_1=-\ell}^{\ell} h_{m_1, b}^{[1,1]} = \sum_{q_1=-\ell}^{\ell} (J_{\mathbf{u}} \mathbf{f}(\mathbf{P}) + \mathbb{D} \nabla^2) \mathbf{W}_{q_1}^{[1,1]} \\ + (\mu - \mu^*) \sum_{q_1=-\ell}^{\ell} \left(\mathbf{G}_{1,1} \left(\mathbf{W}_{q_1,2}^{[1,0]} \right) - \frac{\partial B}{\partial \mu} \mathbf{W}_{q_1,1}^{[1,0]} - \mathbf{W}_{q_1,2}^{[1,0]} - \mathbf{W}_{q_1,1}^{[1,0]} \Big|_{\Gamma} \right) - \frac{\ell(\ell+1)}{R^2} (\mu - \mu^*) \frac{\partial \mathbb{D}}{\partial \mu} \sum_{q_1=-\ell}^{\ell} \mathbf{W}_{q_1}^{[1,0]}. \quad (34)$$

Next, note that (34) can be split for each amplitude, which means that, for each $-\ell \leq q_1 \leq \ell$

$$(J_{\mathbf{u}} \mathbf{f}(\mathbf{P}) + \mathbb{D} \nabla^2) \mathbf{W}_{q_1}^{[1,1]} = \sum_{b=-\ell}^{\ell} \begin{pmatrix} i_\ell(\boldsymbol{\omega} r) \hat{\boldsymbol{\varphi}} \\ \boldsymbol{\varphi} \end{pmatrix} P_\ell^b(\cos(\theta)) e^{ib\phi} h_{q_1, b}^{[1,1]} \\ - A_{q_1} (\mu - \mu^*) \left(\mathbf{G}_{1,1}(\boldsymbol{\varphi}) - \frac{\partial K}{\partial \mu} (\boldsymbol{\varphi} - i_\ell(\boldsymbol{\omega} R) \hat{\boldsymbol{\varphi}}) \right) P_\ell^{q_1}(\cos(\theta)) e^{iq_1\phi} \\ + \frac{\ell(\ell+1)}{R^2} A_{q_1} (\mu - \mu^*) \frac{\partial \mathbb{D}}{\partial \mu} \begin{pmatrix} i_\ell(\boldsymbol{\omega} r) \hat{\boldsymbol{\varphi}} \\ \boldsymbol{\varphi} \end{pmatrix} P_\ell^{q_1}(\cos(\theta)) e^{iq_1\phi}.$$

Again, in this case, we have a solvability condition that can be used to find $h_{q_1, b}^{[1,1]}$ for every pair of integers $-\ell \leq b, q_1 \leq \ell$. In particular, we use the Fredholm alternative with the vector functions ψ_m^* . Note that

$$\begin{aligned} \left\langle (J_{\mathbf{u}} \mathbf{f}(\mathbf{P}) + \mathbb{D} \nabla^2) \mathbf{W}_{q_1}^{[1,1]}, \psi_m^* \right\rangle &= \left\langle \begin{pmatrix} i_\ell(\omega r) \hat{\varphi} \\ \varphi \end{pmatrix} P_\ell^m(\cos(\theta)) e^{im\phi} h_{q_1, m}^{[1,1]}, \psi_m^* \right\rangle \\ &- A_{q_1} (\mu - \mu^*) \left\langle \begin{pmatrix} -\frac{\partial B}{\partial \mu} i_\ell(\omega r) \hat{\varphi} \\ \mathbf{G}_{1,1}(\varphi) - \frac{\partial K}{\partial \mu} (\varphi - i_\ell(\omega R) \hat{\varphi}) \end{pmatrix} P_\ell^{q_1}(\cos(\theta)) e^{iq_1\phi}, \psi_m^* \right\rangle \\ &+ \frac{\ell(\ell+1)}{R^2} A_{q_1} (\mu - \mu^*) \left\langle \frac{\partial \mathbb{D}}{\partial \mu} \begin{pmatrix} i_\ell(\omega r) \hat{\varphi} \\ \varphi \end{pmatrix} P_\ell^{q_1}(\cos(\theta)) e^{iq_1\phi}, \psi_m^* \right\rangle. \end{aligned}$$

Equating this expression to zero, we get $h_{q_1, m}^{[1,1]}(A_m, \mu) = (\mu - \mu^*) C_{1,1} \delta_{q_1, m} A_m$, where

$$\begin{aligned} C_{1,1} &= \frac{1}{I_\ell} \left(\int_0^R \left(-\frac{\partial B}{\partial \mu} i_\ell(\omega r) S_\ell \varphi \right) \cdot (i_\ell(\omega r) S_\ell \psi) r^2 dr \right. \\ &+ R^2 \left(\mathbf{G}_{1,1}(\varphi) - \frac{\partial K}{\partial \mu} (\varphi - i_\ell(\omega R) \hat{\varphi}) \right) \cdot \psi - \frac{\ell(\ell+1)}{R^2} \times \\ &\left. \left(\int_0^R \left(\frac{\partial \mathbb{D}_U}{\partial \mu} i_\ell(\omega r) S_\ell \varphi \right) \cdot (i_\ell(\omega r) S_\ell \psi) r^2 dr + R^2 \left(\frac{\partial \mathbb{D}_u}{\partial \mu} \varphi \right) \cdot \psi \right) \right). \end{aligned} \quad (35)$$

Hence, we get the desired result: the amplitude equation is given by

$$\partial_t \mathbf{A} = C_{1,1} (\mu - \mu^*) \mathbf{A} + \sum_{-\ell \leq q_1, q_2 \leq \ell} \mathbf{C}_{q_1, q_2}^{[2]} A_{q_1} A_{q_2} + h.o.t.,$$

if ℓ is even and the quadratic coefficients are non-zero, and

$$\partial_t \mathbf{A} = C_{1,1} (\mu - \mu^*) \mathbf{A} + \sum_{-\ell \leq q_1, q_2, q_3 \leq \ell} \mathbf{C}_{q_1, q_2, q_3}^{[3]} A_{q_1} A_{q_2} A_{q_3} + h.o.t.,$$

if ℓ is odd or ℓ is even and the quadratic coefficients are zero.

5 Numerical examples

In this section, we present the numerical solutions of two different systems of type (1) and calculate the corresponding amplitude equations given in Theorem 1. As described in detail in the Supplementary Materials B, we use the Implicit-Explicit (IMEX) bulk-surface finite element method (see [20, 22, 38, 35, 37], and references therein) which we implemented using the open-source finite element package, FEniCS [5, 34]. All calculations of the coefficients of the amplitude equations were carried out with a Python code, which is made available [53]. Furthermore, in the same repository, a Mathematica script is available to plot bifurcation diagrams and evaluate the coefficients of the amplitude equations at different bifurcation points.

For each equation, we compute the amplitude equations and provide numerical justification of the predictions of the theory through computation of the simplest patterned states. Exploring the complete dynamics of the amplitude equations and comparing it to the dynamics of full BS-RDE is beyond the scope of the current study.

5.1 Brusselator

As a first example, we consider a bulk-surface system with so-called Brusselator kinetics [43]. See [3] and references therein for some of the consequences on localised pattern formation in the case of sub-critical Turing bifurcations on the real line. One motivation of the present work is to look for analogous structures in the bulk-surface framework. We assume that all nonlinear reactions take place on the surface, while we have linear decaying kinetics in the bulk.

Parameter	R	σ_1	σ_2	α	K_1	K_2	D_1	D_2
Value	1	1	0.1	1	0.005	1	1	1

Table 1: Parameter values fixed for the analysis of the Brusselator.

Specifically, we consider the following bulk-surface system

$$\begin{aligned}
\partial_t U &= -\sigma_1 U + D_1 \nabla_\Omega^2 U, & \text{in } \Omega, \\
\partial_t V &= -\sigma_2 V + D_2 \nabla_\Omega^2 V, & \text{in } \Omega, \\
\partial_t u &= \frac{\alpha}{\delta} - \gamma u + u^2 v - K_1 (u - U|_\Gamma) + \delta^2 \nabla_\Gamma^2 u, & \text{on } \Gamma, \\
\partial_t v &= (\gamma - 1) u - u^2 v - K_2 (v - V|_\Gamma) + \nabla_\Gamma^2 v, & \text{on } \Gamma,
\end{aligned}$$

subject to the Robin boundary conditions

$$D_1 \frac{\partial U}{\partial \hat{\mathbf{n}}}\Big|_\Gamma = K_1 (u - U|_\Gamma), \quad \text{and} \quad D_2 \frac{\partial V}{\partial \hat{\mathbf{n}}}\Big|_\Gamma = K_2 (v - V|_\Gamma), \quad \text{on } \Gamma.$$

We start by looking for radially symmetric steady states. In order to use the same notation we have used throughout this article, let us define $\mathbf{U} = (U, V)^\top$, $\mathbf{u} = (u, v)^\top$, $\mathbf{g}(\mathbf{u}) = \begin{pmatrix} \frac{\alpha}{\delta} - \gamma u + u^2 v \\ (\gamma - 1) u - u^2 v \end{pmatrix}$, $K = \begin{pmatrix} K_1 & 0 \\ 0 & K_2 \end{pmatrix}$, and $\mathbb{D}_u = \begin{pmatrix} \delta^2 & 0 \\ 0 & 1 \end{pmatrix}$. Then, the radially-symmetric steady state is given by $\mathbf{P} = (\mathbf{U}^*(r), \mathbf{u}^*)$, where $\mathbf{U}^*(r) = i_0(\omega r) S_0 \mathbf{u}^*$, and $\mathbf{g}(\mathbf{u}) - K (I - i_0(\omega r) S_0) \mathbf{u}^* = \mathbf{0}$. We fix the non-dimensional parameters given in Table 1, and leave γ and δ as free parameters. Under this choice of parameter values, the system has only one radially symmetric steady state $(\mathbf{U}^*(r), \mathbf{u}^*)$. For this steady state, we get the bifurcation curves shown in Figure 4a in the $\gamma - \delta$ plane. These are the curves determined by the condition $\det \mathbb{B}_\ell = 0$ for different values of ℓ , as shown in the figure. At each point, these curves give rise to the amplitude equations stated in Theorem 1. Note that the radially symmetric steady-state is stable only in the region below and to the left of all the bifurcation curves shown in the figure. To pose the amplitude equations, we use $\varepsilon = C_{1,1} (\mu - \mu^*)$ to simplify notation. We have computed the amplitude equations for the bifurcations occurring at each of the bifurcation points identified by solid dots in the figure. In each case, the coefficients were computed using the code in [53] for which each nonlinear term can take an arbitrary value and they turned out to obey the same form as shown by the theory (see Sec. 3.1 and [12]) without making that assumption *a priori*.

The case $\ell = 1$. When $(\gamma, \delta) = (4.639433, 0.55)$, \mathbf{P} goes through a (Turing) pitchfork bifurcation for $\ell = 1$. The amplitude equations were computed to take the form given in (17), with $a = -0.380329$ and $C_{1,1} = 0.730658$ for $\mu = \gamma$. The manifold of steady states analysed in Sec. 3 is given by

$$\varepsilon = 0.380329 \left(A_0^2 + 2 |A_1|^2 \right). \quad (36)$$

The fact that $a < 0$ implies that this family is stable. Therefore, because of the study in [12] and the equivariant branching lemma [28], we know there must exist a stable small-amplitude pattern right after the bifurcation point.

Now, if we set $(\gamma, \delta) = (5, 0.55)$, then we get the dispersion relation shown in Figure 4b that has $\ell = 1$ as an unstable mode. Furthermore, after setting a random initial condition close to the steady state and integrating the system up to $t = 200$, we find the pattern shown in the top-left panel of Figure 5, which corresponds to solution (a) in Figure 1.

The case $\ell = 2$. When $(\gamma, \delta) = (4.758051, 0.4)$, \mathbf{P} goes through a Turing transcritical bifurcation for $\ell = 2$. Here, the amplitude equations are given by (18) with $a = -0.0132424$ and $C_{1,1} = 0.620246$ for $\mu = \gamma$. As we can see, a has a small magnitude. In fact, there is a nearby codimension-two point for which $a = 0$ at $(\gamma, \delta) = (4.76748, 0.376823)$. At such point, we find $b = 0.173063 > 0$. Therefore, the point marked in Figure

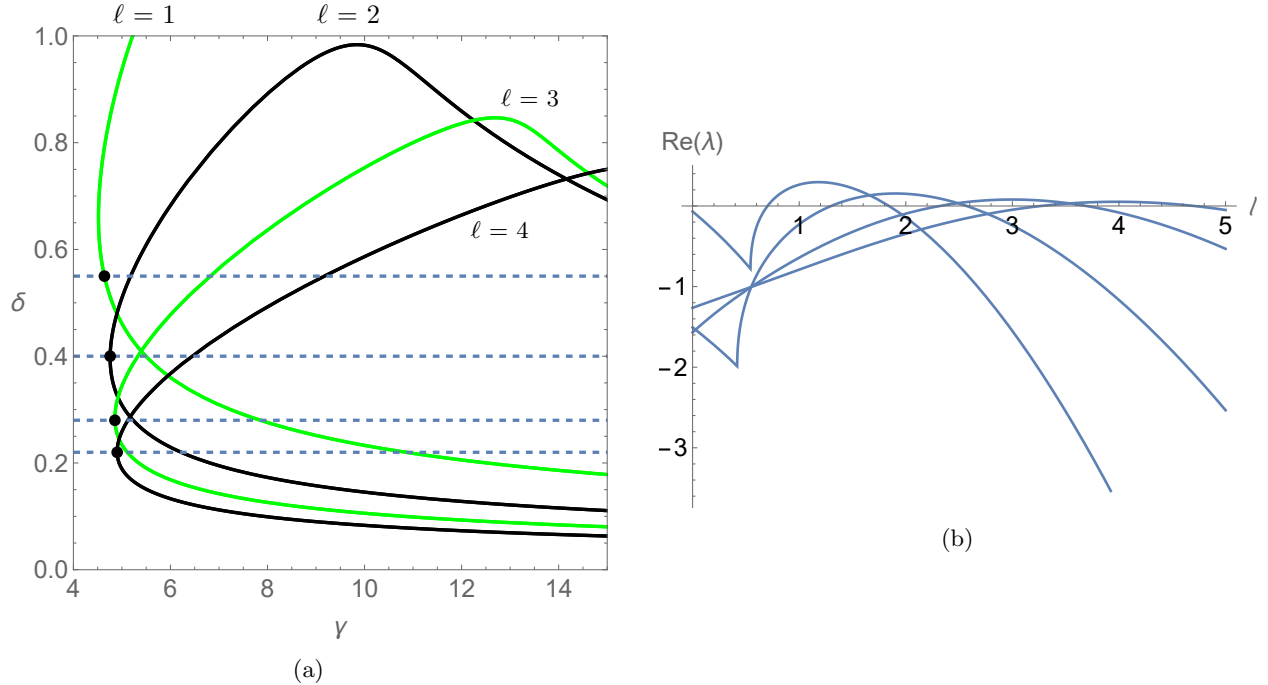


Figure 4: (a) Bifurcation curves at which \mathbf{P} undergoes a Turing bifurcation for different values of γ and δ in the Brusselator, with the parameters in Table 1 fixed. Green (resp. black) curves are (Turing) pitchfork (resp. (Turing) transcritical) bifurcations in the corresponding amplitude equations. (b) Dispersion relation for the Brusselator when the parameters in Table 1 are fixed, $\gamma = 5$, and $\delta \in \{0.55, 0.4, 0.28, 0.22\}$. Here, the unstable value of ℓ increases as δ decreases, according to panel (a).

4a for $\ell = 2$ belongs to Region 1 in the diagram shown in Figure 2. Thus, we expect to see a stable finite-amplitude steady state just after the bifurcation. Once again, we note that all coefficients were obtained using the code in [53]. They follow the same structure as in [12], for the parameter values a and b provided.

After setting $(\gamma, \delta) = (5, 0.4)$, we get the dispersion relation shown in the top-right panel of Figure 4b with $\ell = 2$ as the unstable mode. After integrating the system up to $t = 200$, with a random initial condition close to the steady state, we obtained the pattern shown in the top-right panel of Figure 5. Indeed, the transient numerical simulation leading to this stable pattern was found to show evidence of an initial jump to an intermediate weakly unstable pattern of smaller amplitude. See Supplementary Materials for graphs of transient simulations. Note that the stable pattern comprises two spots on the sides of the sphere together with a stripe in the middle. This corresponds to spherical harmonic Y_2^0 (panel (b) in Fig. 1) as predicted by the theory.

The case $\ell = 3$. When $(\gamma, \delta) = (4.855527, 0.28)$, \mathbf{P} goes through a (Turing) pitchfork bifurcation. Here, the amplitude equations are found to be given by (22) with $a = 0.00128584$, $b = -0.078502$, and $C_{1,1} = 0.551339$ when $\mu = \gamma$. Therefore, we are in Region 1 of the diagram shown in Figure 3 and we expect to see a stable low-amplitude steady state after the bifurcation that resembles spherical harmonic Y_3^2 (panel (c) in Fig. 1). We note that a is close to zero. Thus, if we were to move the parameters a little bit into the region where a is negative (Region 7) then we find a different stable pattern (solution not shown, but it resembles Y_3^3 , the pattern found for $\ell = 3$ in Fig. 7).

Indeed, setting $(\gamma, \delta) = (5, 0.28)$, which is just beyond the bifurcation point, we find the dispersion relation shown in Figure 4b with the mode $\ell = 3$ being unstable. Furthermore, after integrating the system with a random initial condition close to the steady state up to $t = 400$, we found the pattern shown in the bottom-left panel of Figure 5, which indeed corresponds to Y_3^2 as predicted.

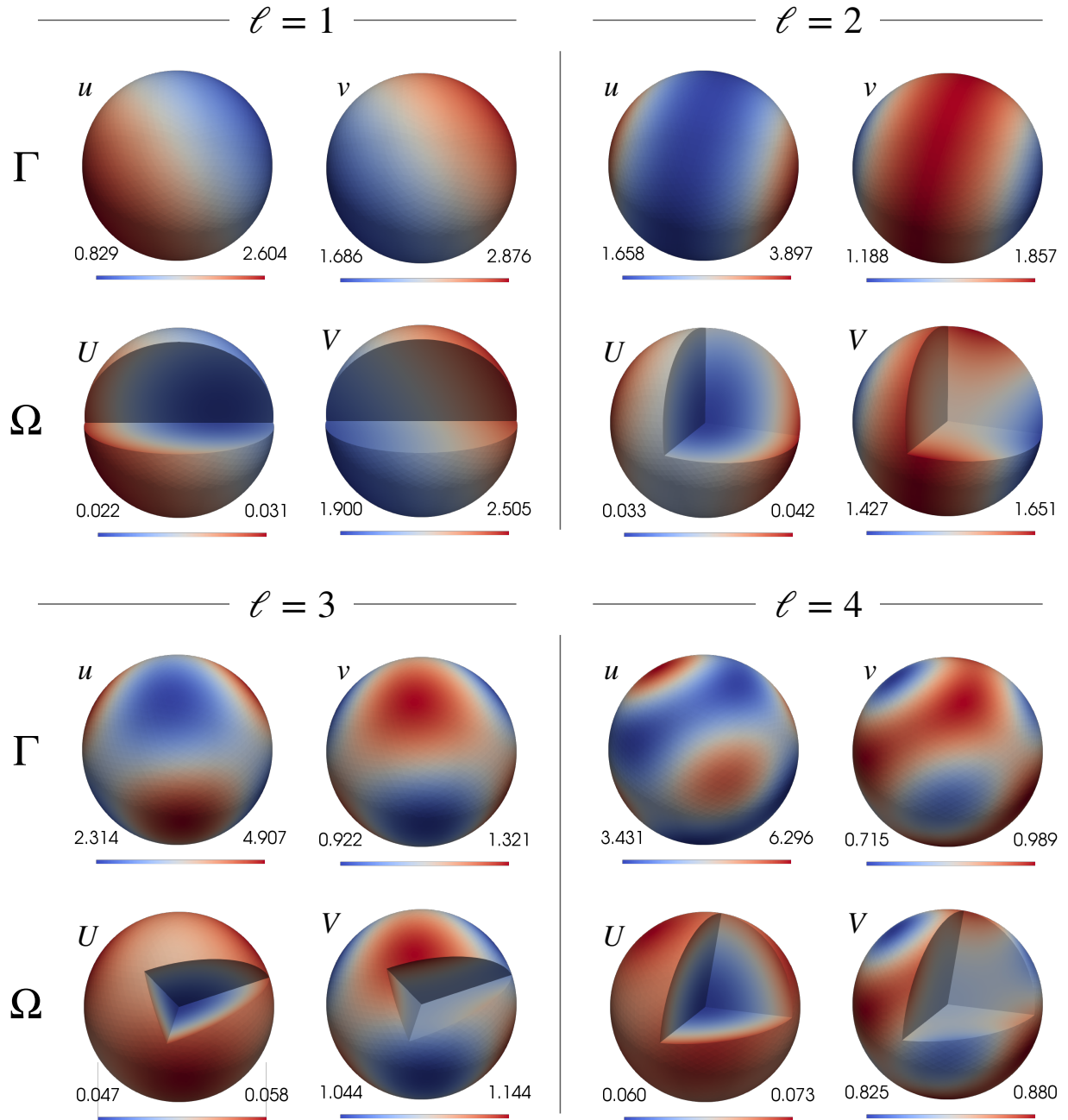


Figure 5: The numerical solutions (u, v, U, V) of the Brusselator system, for four different parameter sets, corresponding to the choices $\ell = 1, 2, 3, 4$, at the corresponding final times, respectively, $t = 200$; $t = 200$; $t = 400$ and $t = 600$.

Parameter	R	σ_1	σ_2	σ_3	σ_4	α	η	θ	μ	ξ
Value	1	100	1	100	1	0.05	3.6	5.5	0.5	2.7
Parameter	ρ	K_1	K_2	K_3	K_4	D_1	D_2	D_3	D_4	δ_2
Value	0.06	1	100	1	100	1	1	1	1	1

Table 2: Parameter values fixed for the analysis of the cell-polarity model.

The case $\ell = 4$. When $(\gamma, \delta) = (4.902346, 0.22)$, \mathbf{P} goes through a (Turing) transcritical bifurcation. In this case, the amplitude equations up to second order are given by (15) with $a = -0.000140359$ and $C_{1,1} = 0.521154$ for $\mu = \gamma$. Again, in this case, we find that a is small and we are close to a codimension-two point for which $a = 0$, which we find to occur at $(\gamma, \delta) = (4.90393, 0.216563)$.

To determine the kind of pattern we expect to see requires the evaluation of cubic coefficients which depend on two independent parameters, b and c (see [12, 18] and Supplementary Materials). We found at the codimension-two point that $b = 0.0000758108$ and $c = -0.0480261$. This can be shown to imply (based on [12, Tables 4-5]) that pattern (f) in Fig. 1 will be the stable branch that emerges from the bifurcation.

To confirm this weakly nonlinear prediction, we set the parameters $(\gamma, \delta) = (5, 0.22)$ for which we get the dispersion relation shown in Figure 4b with the mode $\ell = 4$ being unstable. Moreover, after setting a random initial condition close to the steady state and integrating the system up to $t = 400$, we got the pattern shown in the bottom-right panel of Figure 5. This pattern also comprises spots and stripes as the one in the top-right panel of Figure 5. It corresponds to pattern (f) in Figure 1, as predicted by the theory.

5.2 Cell polarity model

Since we have developed the methodology in a general way, it is useful to consider an example with more than two components. To that end, we present a model analyzed in Chapter 6 of [4]. This is a small modification, through the presence of source and loss terms, to the model developed by Abley *et al* [1] for cellular pattern formation. Here, there are four fields, each of which represents the concentration of a small G-protein, known as an ROP in plants. These ROPs occur in two families with concentrations (u, v) and (w, z) respectively, each of which has an active (u and w) and an inactive (v and z) form. The inactive form is mostly present in the cell body and the active form is on the cell membrane, where the reaction kinetics occurs. Different patterns of the active form are thought to provide the precursor to differential growth; see e.g. [7, 14].

Previous mathematical studies of related systems typically take a homogenization approach within a single lower-dimensional domain, which represents both the bulk and the surface. Here, the system will be posed as

$$\begin{aligned} \partial_t \mathbf{U} &= -B \mathbf{U} + \mathbb{D}_U \nabla_\Omega^2 \mathbf{U}, \quad \text{in } \Omega, \\ \mathbb{D}_U \frac{\partial \mathbf{U}}{\partial \hat{\mathbf{n}}} &= K (\mathbf{u} - \mathbf{U}|_\Gamma), \quad \text{on } \Gamma, \\ \partial_t \mathbf{u} &= \mathbf{g}(\mathbf{u}) - K (\mathbf{u} - \mathbf{U}|_\Omega) + \mathbb{D}_u \nabla_\Gamma^2 \mathbf{u}, \quad \text{on } \Gamma, \quad \text{where} \end{aligned}$$

$$\mathbf{U} = (U, V, W, Z)^\top, \quad \mathbf{u} = (u, v, w, z)^\top, \quad B = \text{diag}(\sigma_1, \sigma_2, \sigma_3, \sigma_4), \\ \mathbb{D}_U = \text{diag}(D_1, D_2, D_3, D_4), \quad K = \text{diag}(K_1, K_2, K_3, K_4),$$

$$\mathbf{g}(\mathbf{u}) = \begin{pmatrix} F(u, v, w, z) - \kappa \xi u \\ -F(u, v, w, z) + \kappa \theta \\ G(u, v, w, z) - \kappa \xi w \\ -G(u, v, w, z) + \kappa \theta \end{pmatrix}, \quad \mathbb{D}_u = \text{diag}(\delta_1^2, 1, \delta_2^2, 1), \quad \text{and}$$

$$F(u, v, w, z) = (\eta u^2 + \rho) v - (\alpha w + \mu) u, \quad \text{and} \quad G(u, v, w, z) = (\eta w^2 + \rho) z - (\alpha u + \mu) w.$$

We find that although the calculation of the coefficients of the amplitude equations takes more time, the normal forms have the same form as the ones in the previous example, as predicted by the equivariant bifurcation theory. For illustration, we consider the parameter values shown in Table 2 which are indicative rather than precise values for any particular biological system. Here, we leave δ_1 and κ as free parameters. As usual, we start by computing bifurcation curves and dispersion relations for different values of ℓ . Figure 6a shows the corresponding neutral stability curves in the (κ, δ_1) plane.

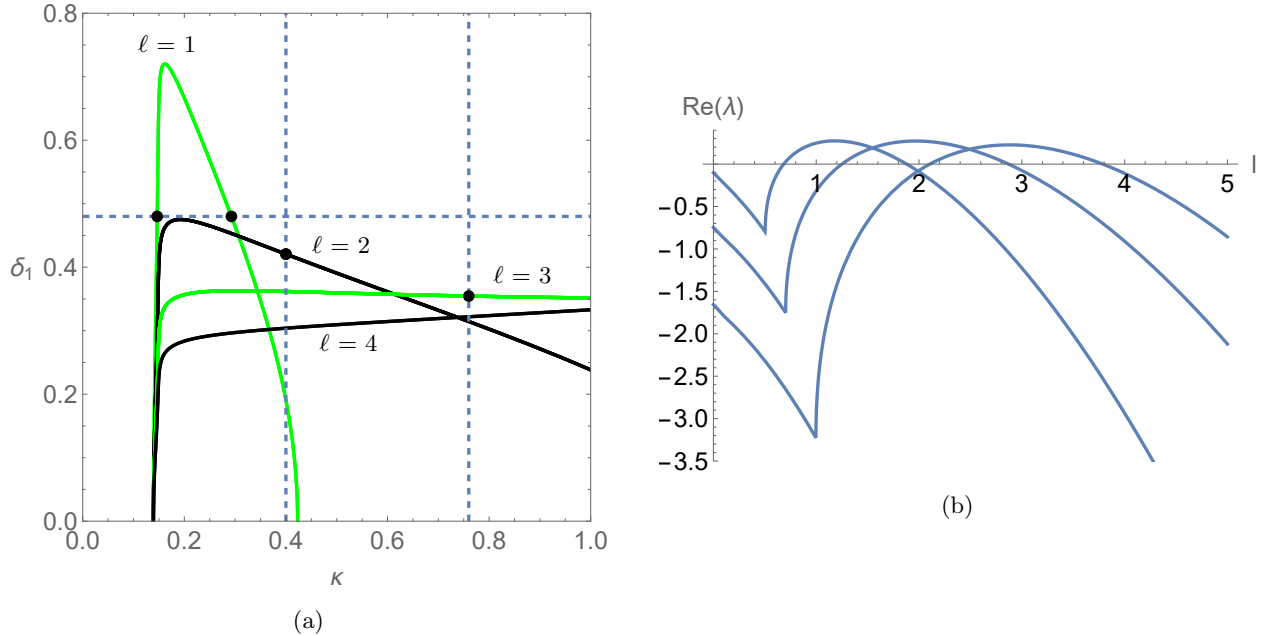


Figure 6: (a) Bifurcation curves for the cell polarity model at one steady state when the parameters in Table 2 are fixed. Green (resp. black) curves are pitchfork (resp. transcritical) bifurcations in the corresponding amplitude equations. (b) Dispersion relations for $(\kappa, \delta_1) \in \{(0.25, 0.48), (0.4, 0.37), (0.76, 0.33)\}$.

The case $\ell = 1$. When $(\kappa, \delta_1) = (0.292672, 0.48)$, there is a bifurcation for $\ell = 1$, with the amplitude equations given by (17) with $a = 1.6352 > 0$ and $C_{1,1} = -6.30308$ for $\mu = \kappa$. On the other hand, when $(\kappa, \delta_1) = (0.146644, 0.48)$, the same happens with $a = 160.42 > 0$ and $C_{1,1} = 112.596$ for $\mu = \kappa$. This implies that we do not expect to see a stable pattern when integrating the solution when $\delta_1 = 0.48$ and $0.146644 < \kappa < 0.48$ is sufficiently close to these bifurcation points. Figure 6b shows the dispersion relation obtained for $(\kappa, \delta_1) = (0.25, 0.48)$, which is in the interior of the region in which the $\ell = 1$ mode is the only unstable one. Furthermore, when integrating the system from a random perturbation to the ground state, we do not see a stable steady state. Instead, the solution seems to converge to a periodic orbit. One state of the solution is shown in the first and second rows of Figure 7 for a fixed time instant. It is clear from the temporal evolution that the simulation quickly settles to a limit cycle (see the L^2 -norm of Figure 12, shown within the supplementary material and the associated video there).

The case $\ell = 2$. When $(\kappa, \delta_1) = (0.4, 0.420644)$, there is a bifurcation for $\ell = 2$ that gives rise to amplitude equations given by (18) with $a = 0.0414126$ and $C_{1,1} = -5.81929$ for $\mu = \delta_1$. Here, we are indeed close to a codimension-two bifurcation point. In fact, there is a codimension-two point for $(\kappa, \delta_1) = (0.362182, 0.432158)$, at which $b = 1.15796 > 0$. Therefore, we expect to see a stable moderate-amplitude steady state close to the bifurcation. The dispersion relation obtained for $(\kappa, \delta_1) = (0.4, 0.37)$ is shown in Figure 6b. Furthermore, the pattern obtained after integrating the system at these parameter values from a random perturbation to the steady state \mathbf{P} is shown in the third and fourth rows of Figure 7.

The case $\ell = 3$. When $(\kappa, \delta_1) = (0.76, 0.354603)$, there is a bifurcation associated with $\ell = 3$ that gives rise to amplitude equations that look like (22) with $a = -0.0252879$, $b = -1.03659$ and $C_{1,1} = -9.44413$ for $\mu = \delta_1$. Therefore, we are in Region 7 on the diagram shown in Figure 3, which makes us expect pattern (d) in Figure 1 to become stable right after the bifurcation. The dispersion relation obtained for $(\kappa, \delta_1) = (0.76, 0.33)$ is shown in Figure 6b. The pattern obtained after integrating the system at these parameter values from a random small perturbation to the steady state \mathbf{P} is shown in the last two rows of Figure 7.

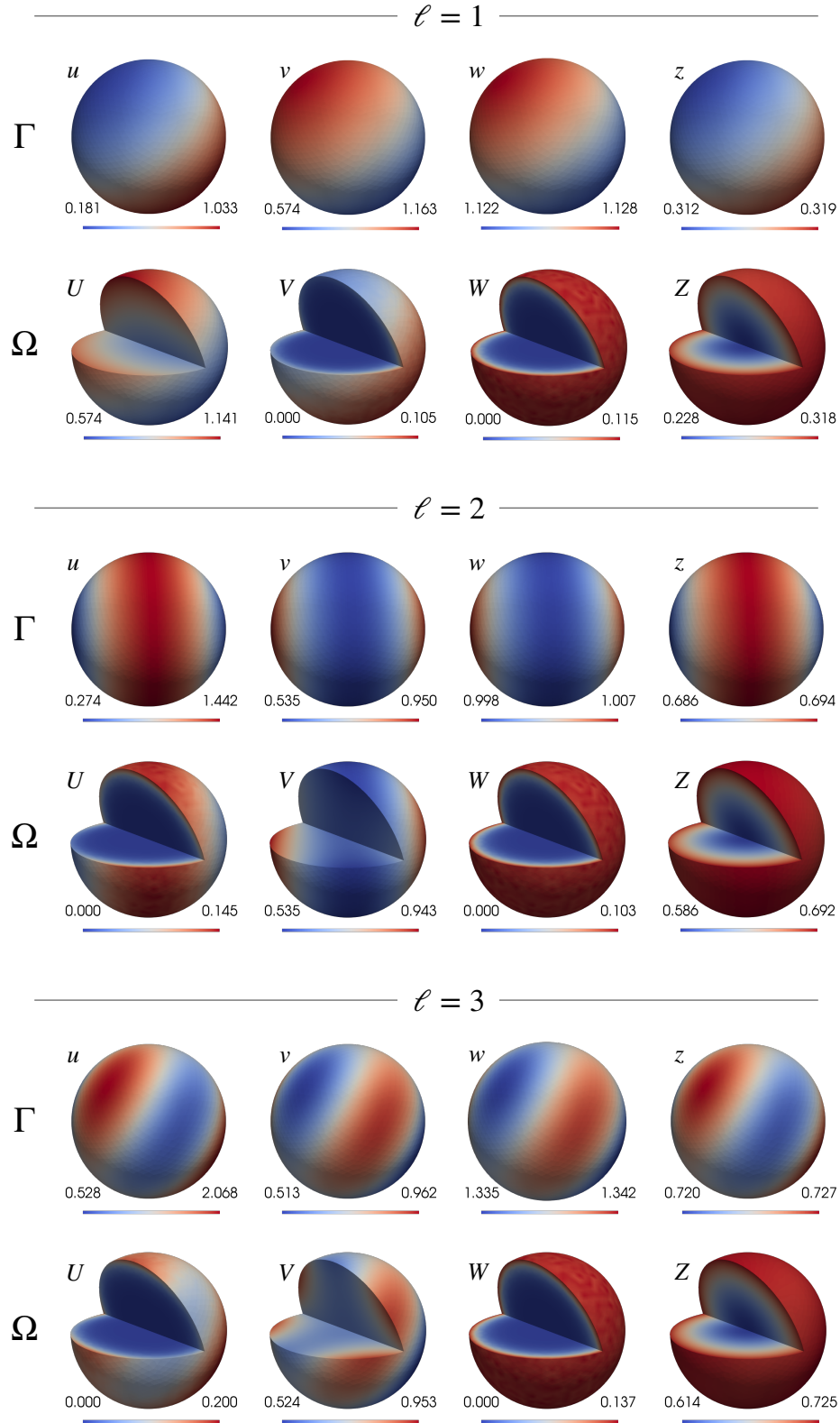


Figure 7: The numerical solutions of the cell polarity system at time $t = 170$, for three different parameter sets, corresponding to the choices $\ell = 1, 2, 3$. For each case, the surface solutions u, v, w, z are plotted in the first row, while the bulk solutions U, V, W, Z are in the second one. Note that the solution for $\ell = 1$ is not at steady state, whereas the other two cases are (see text for details).

6 Conclusion

In this paper, we have provided a method for computing the linear and nonlinear parameters necessary for analysing (Turing) transcritical and pitchfork bifurcations for a broad class of bulk-surface reaction-diffusion systems posed on a sphere. In particular, we consider the physically realistic case where the nonlinear interaction kinetics occurs on the surface, with linear diffusion and decay in the bulk, coupled by a boundary condition that has a natural interpretation in terms of concentration-driven flux.

Compared with bifurcations in planar geometries, the amplitude equations are a little harder to analyze in the case studied because of the $O(3)$ -symmetry of the sphere [28]. Without making an *a priori* assumption, we find that the coefficients follow the normal forms predicted by the theory of such symmetry-breaking [12, 18]. Our main contribution then is to show how to calculate such normal forms for our class of bulk-surface systems. Moreover, we have provided software implementation of this general method [53]. We have also backed-up our theory with computational results using a state-of-the-art finite element method.

Note, however, that we have not fully explored the stability of steady solutions that can exist, especially for higher than $\ell = 1, 2$, as the number of components of the amplitude equations becomes prohibitive. Nevertheless, we have been able to calculate whether the primary bifurcation is super or sub-critical. There has been recent interest in sub-critical bifurcations and how they can lead to localised structures, see e.g. [3, 52, 15, 11] and references therein. The analogy of such states in bulk-surface systems remains unexplored.

We have also not undertaken any investigation of possible spatiotemporal states. All computational results we present are from numerical integration carried out sufficiently close to the bifurcation curve so that the simplest consequences of the normal forms. However, there is still more to do far away from bifurcation curves, as can be seen in the video provided in the supplementary material, which shows a much more complicated transient for different parameter values of the cell-polarity example. Here, we see structures that resemble localised spots that appear meta-stably before the solution eventually collapses back to a much more uniform pattern.

Perhaps some of the spatiotemporal behaviour, including the periodic orbit we observed for $\ell = 1$ in the cell polarity model, may be explainable by studying the complete dynamics of the relevant normal form. Also, we established that the normal forms arising at each kind of bifurcation have several symmetries, with consequent invariant subspaces. For $\ell > 1$ it is therefore likely that we will see parameter regimes where there are robust heteroclinic cycles [32], as has been observed for other amplitude equations, for example the complex Ginzberg-Landau equation in 1D [33].

Finally, we remark on how the method developed in this paper could be adapted to provide amplitude equations for bulk-surface reaction-diffusion systems in other geometries. The case of the sphere with linear kinetics in the bulk was tractable because of the compatibility of the eigenfunctions of the Laplace and Laplace-Beltrami operators in the bulk and on the surface. This enables nonlinear terms arising from products to be expressed in terms of the same eigenbases, leading to closed-form expressions for the required amplitude-equation coefficients. Nevertheless, the approach is general and extensions to other geometries may well be possible provided a suitable alternative to Lemma 2 can be established for that geometry.

Acknowledgments

The authors acknowledge helpful conversations with Alastair Rucklidge (Leeds, UK), Michael Ward (UBC, Canada) and Frédéric Paquin-Lefebvre (Ecole Normal Supérieure, Paris). The work of EV-S was supported by ANID, Beca Chile Doctorado en el extranjero, number 72210071. DC was supported by the “Fundação para a Ciência e a Tecnologia (FCT)” under the projects with reference UIDB/00208/2020 and UIDP/00013/2020. AM was supported by a Canada Research Chair (CRC-2022-00147), the Natural Sciences and Engineering Research Council of Canada (NSERC), Discovery Grants Program (RGPIN-2023-05231), the British Columbia Knowledge Development Fund (BCKDF), Canada Foundation for Innovation – John R. Evans Leaders Fund – Partnerships (CFI-JELF), the UKRI Engineering and Physical Sciences Research Council (EPSRC: EP/J016780/1) and the British Columbia Foundation for Non-Animal Research.

References

- [1] Katie Abley, Pierre Barbier De Reuille, David Strutt, Andrew Bangham, Przemyslaw Prusinkiewicz, Athanasius FM Marée, Verónica A Grieneisen, and Enrico Coen. An intracellular partitioning-based framework for tissue cell polarity in plants and animals. Development, 140(10):2061–2074, 2013.
- [2] Milton Abramowitz and Irene A Stegun. Handbook of Mathematical Functions with Formulas, Graphs, and Mathematical Tables. National Bureau of Standards Applied Mathematics Series 55. Tenth Printing. ERIC, 1972.
- [3] F. Al Saadi, A. Champneys, and N. Verschueren. Localized patterns and semi-strong interaction, a unifying framework for reaction–diffusion systems. IMA Journal of Applied Mathematics, 86(5):1031–1065, 2021.
- [4] Fahad S Al Saadi. Localised structures in reaction-diffusion equations. PhD thesis, University of Bristol, 2022.
- [5] Martin Alnæs, Jan Blechta, Johan Hake, August Johansson, Benjamin Kehlet, Anders Logg, Chris Richardson, Johannes Ring, Marie E Rognes, and Garth N Wells. The fenics project version 1.5. Archive of Numerical Software, 3(100), 2015.
- [6] Amal Alphonse, Charles M Elliott, and Joana Terra. A coupled ligand-receptor bulk-surface system on a moving domain: well posedness, regularity, and convergence to equilibrium. SIAM Journal on Mathematical Analysis, 50(2):1544–1592, 2018.
- [7] C. Beta, L. Eldestein-Keshet, N. Gov, and A. Yochelis. From actin waves to mechanism and back: How theory aids biological understanding. eLife, 12:e87181, 2023.
- [8] Johannes Borgqvist, Adam Malik, Carl Lundholm, Anders Logg, Philip Gerlee, and Marija Cvijovic. Cell polarisation in a bulk-surface model can be driven by both classic and non-classic turing instability. NPJ systems biology and applications, 7(1):13, 2021.
- [9] Jason J Bramburger, Dan J Hill, and David JB Lloyd. Localized multi-dimensional patterns. arXiv preprint arXiv:2404.14987, 2024.
- [10] Fridtjof Brauns, Grzegorz Pawlik, Jacob Halatek, Jacob Kerssemakers, Erwin Frey, and Cees Dekker. Bulk-surface coupling identifies the mechanistic connection between min-protein patterns in vivo and in vitro. Nature Communications, 12(1):3312, 2021.
- [11] John Burke and Edgar Knobloch. Homoclinic snaking: structure and stability. Chaos: An Interdisciplinary Journal of Nonlinear Science, 17(3), 2007.
- [12] TK Callahan. Turing patterns with $o(3)$ symmetry. Physica D: Nonlinear Phenomena, 188(1-2):65–91, 2004.
- [13] A. Champneys. Editorial to Homoclinic snaking at 21: in memory of Patrick Woods. IMA Journal of Applied Mathematics, 86:845–855, 2021.
- [14] A.R. Champneys, F. Al Saadi, V. Breña-Medina, V.A. Grieneisen, A.F.M. Marée, N. Verschueren, and B. Wuyts. Bistability, wave pinning and localisation in natural reaction-diffusion systems. Physica D., 416:art. no. 132735, 2021.
- [15] S Jon Chapman and Gregory Kozyreff. Exponential asymptotics of localised patterns and snaking bifurcation diagrams. Physica D: Nonlinear Phenomena, 238(3):319–354, 2009.
- [16] Laurent Charette and Wayne Nagata. Bifurcation of mixed mode reaction–diffusion patterns in spherical caps. International Journal of Bifurcation and Chaos, 28(06):1830017, 2018.
- [17] Kuan-Yu Chen and Ming-Chih Lai. A conservative scheme for solving coupled surface-bulk convection–diffusion equations with an application to interfacial flows with soluble surfactant. Journal of Computational Physics, 257:1–18, 2014.

- [18] P. Chossat, R. Lauterbach, and I. Melbourne. Steady-state bifurcation with 0 (3)-symmetry. Archive for Rational Mechanics and Analysis, 113:313–376, 1991.
- [19] Richard Courant and David Hilbert. Methods of mathematical physics: partial differential equations. John Wiley & Sons, 2008.
- [20] Davide Cusceddu, Leah Edelstein-Keshet, John A Mackenzie, Stéphanie Portet, and Anotida Madzvamuse. A coupled bulk-surface model for cell polarisation. Journal of theoretical biology, 481:119–135, 2019.
- [21] Davide Cusceddu and Anotida Madzvamuse. Numerical investigations of the bulk-surface wave pinning model. Mathematical Biosciences, 354:108925, 2022.
- [22] Charles M Elliott and Thomas Ranner. Finite element analysis for a coupled bulk–surface partial differential equation. IMA Journal of Numerical Analysis, 33(2):377–402, 2013.
- [23] Charles M Elliott, Thomas Ranner, and Chandrasekhar Venkataraman. Coupled bulk-surface free boundary problems arising from a mathematical model of receptor-ligand dynamics. SIAM Journal on Mathematical Analysis, 49(1):360–397, 2017.
- [24] Christian Elphick, Enrique Tirapegui, ME Brachet, Pierre Coulet, and Gérard Iooss. A simple global characterization for normal forms of singular vector fields. Physica D: Nonlinear Phenomena, 29(1-2):95–127, 1987.
- [25] Lawrence C Evans. Partial differential equations, volume 19. American Mathematical Soc., 2010.
- [26] JR Fernández, Piotr Kalita, Stanislaw Migórski, M Carmen Muñoz, and C Núñez. Existence and uniqueness results for a kinetic model in bulk-surface surfactant dynamics. SIAM Journal on Mathematical Analysis, 48(5):3065–3089, 2016.
- [27] Massimo Frittelli, Ivonne Sgura, and Benedetto Bozzini. Turing patterns in a 3d morpho-chemical bulk-surface reaction-diffusion system for battery modeling. Mathematics in Engineering, 6(2):363–393, 2024.
- [28] Martin Golubitsky, Ian Stewart, and David G Schaeffer. Singularities and Groups in Bifurcation Theory: Volume II, volume 69. Springer Science & Business Media, 2012.
- [29] Nail A Gumerov and Ramani Duraiswami. Fast multipole methods for the Helmholtz equation in three dimensions. Elsevier, 2005.
- [30] Andreas Hahn, Kristin Held, and Lutz Tobiska. Modelling of surfactant concentration in a coupled bulk surface problem. PAMM, 14(1):525–526, 2014.
- [31] A.L. Krause, Gaffney E.A., P.K. Maini, and Klika V. Introduction to ‘Recent progress and open frontiers in Turing’s theory of morphogenesis’. Phil. Trans. R. Soc. Lond. A, 379:20200280, 2021.
- [32] M. Krupa. Robust heteroclinic cycles. J, Nonlinear Sci., 7:129–176, 1997.
- [33] A.R. Lloyd, D.J.B.and Champneys and R.E. Wilson. Robust heteroclinic cycles in the one-dimensional complex ginzburg-landau equation. Physica D, 204:240–268, 2005.
- [34] Anders Logg, Kent-Andre Mardal, and Garth Wells. Automated solution of differential equations by the finite element method: The FEniCS book, volume 84. Springer Science & Business Media, 2012.
- [35] G MacDonald, John A Mackenzie, M Nolan, and RH Insall. A computational method for the coupled solution of reaction–diffusion equations on evolving domains and manifolds: Application to a model of cell migration and chemotaxis. Journal of computational physics, 309:207–226, 2016.
- [36] Anotida Madzvamuse. Time-stepping schemes for moving grid finite elements applied to reaction–diffusion systems on fixed and growing domains. Journal of Computational Physics, 214(1):239–263, 2006.

- [37] Anotida Madzvamuse and Andy HW Chung. The bulk-surface finite element method for reaction–diffusion systems on stationary volumes. Finite Elements in Analysis and Design, 108:9–21, 2016.
- [38] Anotida Madzvamuse, Andy HW Chung, and Chandrasekhar Venkataraman. Stability analysis and simulations of coupled bulk-surface reaction–diffusion systems. Proceedings of the Royal Society A: Mathematical, Physical and Engineering Sciences, 471(2175):20140546, 2015.
- [39] PC Matthews. Pattern formation on a sphere. Physical Review E, 67(3):036206, 2003.
- [40] PC Matthews. Transcritical bifurcation with $o(3)$ symmetry. Nonlinearity, 16:1449–1471, 2003.
- [41] J. Murdock. Normal Forms and Unfoldings for Local Dynamical Systems. Springer, New York, 2003.
- [42] Frédéric Paquin-Lefebvre, Wayne Nagata, and Michael J Ward. Pattern formation and oscillatory dynamics in a two-dimensional coupled bulk-surface reaction-diffusion system. SIAM Journal on Applied Dynamical Systems, 18(3):1334–1390, 2019.
- [43] I. Prigogine and R. Lefever. Symmetry breaking instabilities in dissipative systems. 2. J. Chem. Phys., 48:1695–1700, 1968.
- [44] Alfio Quarteroni and Alberto Valli. Numerical approximation of partial differential equations, volume 23. Springer Science & Business Media, 2008.
- [45] Andreas Rätz. Turing-type instabilities in bulk–surface reaction–diffusion systems. Journal of computational and applied mathematics, 289:142–152, 2015.
- [46] Andreas Rätz and Matthias Röger. Symmetry breaking in a bulk–surface reaction–diffusion model for signalling networks. Nonlinearity, 27(8):1805, 2014.
- [47] Steven J Ruuth. Implicit-explicit methods for reaction-diffusion problems in pattern formation. Journal of Mathematical Biology, 34(2):148–176, 1995.
- [48] Sandro Salsa. Partial differential equations in action: from modelling to theory, volume 99. Springer, 2016.
- [49] Amit R Singh, Travis Leadbetter, and Brian A Camley. Sensing the shape of a cell with reaction diffusion and energy minimization. Proceedings of the National Academy of Sciences, 119(31):e2121302119, 2022.
- [50] Steven H Strogatz. Nonlinear dynamics and chaos with student solutions manual: With applications to physics, biology, chemistry, and engineering. CRC press, 2018.
- [51] Alan Mathison Turing. The chemical basis of morphogenesis. Bulletin of mathematical biology, 52(1):153–197, 1990.
- [52] Edgardo Villar-Sepúlveda and Alan Champneys. Degenerate turing bifurcation and the birth of localized patterns in activator-inhibitor systems. SIAM Journal on Applied Dynamical Systems, 22(3):1673–1709, 2023.
- [53] Edgardo Villar-Sepúlveda. Amplitude equations in bulk-surface RD equations.

Supplementary materials

A Proof of Lemma 1

For (19), note that

$$\begin{aligned}
\frac{d}{dt} \left(|A_2|^2 - \frac{3}{2} A_0^2 \right) &= \dot{A}_{-2} A_2 + A_{-2} \dot{A}_2 - 3 A_0 \dot{A}_0 \\
&= A_{-2} (\varepsilon + 4 a A_0) A_2 \\
&\quad + A_{-2} A_2 (\varepsilon + 4 a A_0) \\
&\quad - 3 A_0 (A_0 (\varepsilon - 2 a A_0) + 4 a A_{-2} A_2) \\
&= 2 |A_2|^2 (\varepsilon + 4 a A_0) \\
&\quad - 3 \left(A_0^2 (\varepsilon - 2 a A_0) + 4 a A_0 |A_2|^2 \right) \\
&= 0.
\end{aligned}$$

On the other hand, to analyze (20), note that $\dot{A}_0 = 0$ trivially, by the conditions that set the manifold. Furthermore,

$$\begin{aligned}
\frac{d}{dt} \left(2 |A_2|^2 - |A_1|^2 \right) &= 2 \left(\dot{A}_{-2} A_2 + A_{-2} \dot{A}_2 \right) + \dot{A}_{-1} A_1 + A_{-1} \dot{A}_1 \\
&= 2 \left(\left(\varepsilon A_{-2} - \sqrt{6} a A_{-1}^2 \right) A_2 \right. \\
&\quad \left. + A_{-2} \left(\varepsilon A_2 - \sqrt{6} a A_1^2 \right) \right) \\
&\quad + \left(\varepsilon A_{-1} + 2 \sqrt{6} a A_1 A_{-2} \right) A_1 \\
&\quad + A_{-1} \left(\varepsilon A_1 + 2 \sqrt{6} a A_{-1} A_2 \right) \\
&= 2 \left(2 \varepsilon |A_2|^2 - \sqrt{6} a A_{-1}^2 A_2 - \sqrt{6} a A_{-2} A_1^2 \right) \\
&\quad - 2 \varepsilon |A_1|^2 + 2 \sqrt{6} a A_1^2 A_{-2} + 2 \sqrt{6} a A_{-1}^2 A_2 \\
&= 0.
\end{aligned}$$

Finally, to analyze (21), note that if we subtract the first two equations, we get

$$\dot{A}_0 = A_0 (\varepsilon - 2 a A_0) - 2 a |A_1|^2 + 4 a |A_2|^2 = 0.$$

Therefore, due to the last equation in (21), we have that A_0 and A_2 are constants fulfilling

$$4 A_0 \left(-A_0 + \frac{\varepsilon}{a} \right) + 24 |A_2|^2 = \frac{\varepsilon^2}{a^2}.$$

Now, note that

$$\begin{aligned}
\dot{A}_1 &= A_1 (\varepsilon - 2 a A_0) + 2 \sqrt{6} a A_{-1} A_2 = A_1 (\varepsilon - 2 a A_0) + 2 \sqrt{6} a A_{-1} \frac{\sqrt{6} a A_1^2}{\varepsilon + 4 a A_0} \\
&= A_1 \frac{(\varepsilon - 2 a A_0) (\varepsilon + 4 a A_0) + 12 a^2 A_{-1} A_1}{\varepsilon + 4 a A_0} \\
&= 0
\end{aligned}$$

Therefore, the right-hand side of all the equations in (18) are equal to zero. That implies that all the variables are constants in the manifold determined by (21), which concludes the proof.

B The numerical scheme

As a complement to our analytical results, we present and discuss the numerical solutions of some examples of bulk-surface systems of type (1). We solve such systems by employing the bulk-surface element method, which has been developed and used in the literature for studying different systems, often arising from modelling real-world phenomena, such as cell polarisation and migration, see e.g. [38, 20, 22, 35, 37]. Before outlining the procedure for the specific system (1), we rewrite the system in a more explicit form. Specifically, we write

$$\frac{\partial U_p}{\partial t} = -\sigma_p U_p + D_p \nabla_{\Omega}^2 U_p, \quad \text{in } \Omega, \quad (37)$$

$$D_p \frac{\partial U_p}{\partial \nu} = K_p (u_p - U_p), \quad \text{on } \Gamma, \quad (38)$$

$$\frac{\partial u_p}{\partial t} = g_p(u_1, \dots, u_n) - K_p u_p + K_p U_p + d_p \nabla_{\Gamma}^2 u_p, \quad \text{on } \Gamma, \quad (39)$$

for $p = 1, \dots, n$. In what follows we assume $g_p \in L^2(\mathbb{R}^n)$ for all $p = 1, \dots, n$. Let Φ_p and ϕ_p be functions of the Sobolev spaces $H^1(\Omega)$ and $H^1(\Gamma)$, respectively. The following weak formulation of the above problem is derived by testing (37) with Φ_p and applying the boundary condition (38), and by testing (39) with ϕ_p . It must be noted that the surface equation (39) has no boundary conditions since Γ is a closed surface.

Hence, the bulk-surface finite element method seeks to: Find $(U_1, \dots, U_n) \in L^2([0, T]; H^1(\Omega)) \cap L^\infty([0, T] \times \Omega)$, with

$$\left(\frac{\partial U_1}{\partial t}, \dots, \frac{\partial U_n}{\partial t} \right) \in L^2([0, T]; H^{-1}(\Omega))$$

and $(u_1, \dots, u_n) \in L^2([0, T]; H^1(\Gamma)) \cap L^\infty([0, T] \times \Gamma)$ with

$$\left(\frac{\partial u_1}{\partial t}, \dots, \frac{\partial u_n}{\partial t} \right) \in L^2([0, T]; H^{-1}(\Gamma)),$$

such that, $\forall \Phi_p \in H^1(\Omega)$ and $\forall \phi_p \in H^1(\Gamma)$, these functions satisfy

$$\begin{aligned} \int_{\Omega} \frac{\partial U_p}{\partial t} \Phi_p \, d\mathbf{x} &= - \int_{\Omega} \sigma_p U_p \Phi_p \, d\mathbf{x} - D_p \int_{\Omega} \nabla_{\Omega} U_p \cdot \nabla_{\Omega} \Phi_p \, d\mathbf{x} \\ &\quad + K_p \int_{\Gamma} (u_p - U_p) \Phi_p \, ds, \end{aligned} \quad (40)$$

$$\begin{aligned} \int_{\Gamma} \frac{\partial u_p}{\partial t} \phi_p \, ds &= \int_{\Gamma} g_p(u_1, \dots, u_n) \phi_p \, ds - K_p \int_{\Gamma} (u_p - U_p) \phi_p \, ds \\ &\quad - d_p \int_{\Gamma} \nabla_{\Gamma} u_p \cdot \nabla_{\Gamma} \phi_p \, ds, \end{aligned} \quad (41)$$

with $U_p(0, \mathbf{x}) = U_{p,0}(\mathbf{x})$ and $u_p(0, \mathbf{x}) = u_{p,0}(\mathbf{x})$ as prescribed by the initial conditions to (37)-(39), for $p = 1, \dots, n$. The spaces $L^2([0, T]; H^1(\Omega))$ and $L^2([0, T]; H^1(\Gamma))$ are known as Bochner spaces and $H^{-1}(\Omega)$ and $H^{-1}(\Gamma)$ are the dual space of, respectively, $H^1(\Omega)$ and $H^1(\Gamma)$ [25, 48].

B.1 Spatial discretisation

The bulk-surface finite element method (BS-FEM) is based on a restriction of the above weak formulation to discrete function spaces. First, let Ω_h be a polyhedral approximation of the domain Ω and $\Gamma_h = \partial\Omega_h$ its boundary. Let $\mathcal{T}_h = \{T_1, \dots, T_{n_x(h)}\}$ be a mesh on Ω_h , i.e. a set of polyhedrons whose intersection is either empty or a polygonal face and such that $\bigcup_{i=1}^{n_x(h)} T_i = \Omega_h$ (for details on proper choices of such elements see, e.g., [44]). By considering the set $\mathcal{S}_h = \{T_i \cap \Gamma_h, \text{ for } i = 1, \dots, n_x(h)\}$ which is constituted by polygons, i.e. by the faces of the elements of \mathcal{T}_h relying on the boundary Γ_h , we naturally define a mesh on Γ_h entirely induced by \mathcal{T}_h . Therefore, by choosing tetrahedron elements T_i , the mesh Γ_h will be constituted by triangles. Let N_{Ω} and N_{Γ} denote the number

of total vertices in the bulk and surface meshes, respectively. These meshes help us in defining appropriate basis functions for deriving the BS-FEM. Let us define the following function spaces

$$\begin{aligned} V_h(\Omega_h) &:= \left\{ \Phi_h : \Omega_h \rightarrow \mathbb{R} \text{ such that } \Phi_h \in C^0(\Omega_h) \text{ and } \Phi_h|_T \in \mathbb{P}_1(T), \forall T \in \mathcal{T}_h \right\}, \\ W_h(\Gamma_h) &:= \left\{ \phi_h : \Gamma_h \rightarrow \mathbb{R} \text{ such that } \phi_h \in C^0(\Gamma_h) \text{ and } \phi_h|_S \in \mathbb{P}_1(S), \forall S \in \mathcal{S}_h \right\}, \end{aligned}$$

where $\mathbb{P}_1(D)$ indicates the space of all linear polynomials over a domain D . In particular, $V_h(\Omega_h) \subset H^1(\Omega_h)$ and $W_h(\Gamma_h) \subset H^1(\Gamma_h)$. Basis functions for these two spaces are, respectively, $(\Psi_i(\mathbf{x}))_{i=1, \dots, N_\Omega} \in [V_h(\Omega_h)]^{N_\Omega}$ and $(\psi_i(\mathbf{x}))_{i=1, \dots, N_\Gamma} \in [W_h(\Gamma_h)]^{N_\Gamma}$ with the property $\Psi_i(\mathbf{x}_j) = \delta_{i,j}$ for all vertices \mathbf{x}_j of the mesh $\mathcal{T}_h(\Omega_h)$ ($j = 1, \dots, N_\Omega$) and $\psi_i(\mathbf{x}_k) = \delta_{i,k}$ for all vertices \mathbf{x}_k of $\mathcal{S}_h(\Gamma_h)$ ($k = 1, \dots, N_\Gamma$). Here, $\delta_{i,j}$ is the Kronecker delta.

Thanks to the basis functions, our problem goes from looking for functions over the time-space domain to look for solely time-dependent functions $A_i^p(t)$ and $a_k^p(t)$ such that $U_{h,p}(t, \mathbf{x}) = \sum_i A_i^p(t) \Psi_i(\mathbf{x})$ and $u_{h,p}(t, \mathbf{x}) = \sum_i a_i^p(t) \psi_i(\mathbf{x})$ for $p = 1, \dots, n$. Therefore, the semi-discrete weak formulation reads as follows.

Find $A_i^p \in \mathbb{R}$ for $i = 1, \dots, N_\Omega$ and $a_k^p \in \mathbb{R}$ for $k = 1, \dots, N_\Gamma$ and $p = 1, \dots, n$ such that

$$\begin{aligned} \sum_{i=1}^{N_\Omega} \frac{dA_i^p}{dt} \int_{\Omega_h} \Psi_i \Psi_j \, d\mathbf{x} &= -\sigma_p \sum_{i=1}^{N_\Omega} A_i^p(t) \int_{\Omega_h} \Psi_i \Psi_j \, d\mathbf{x} \\ &\quad - D_p \sum_{i=1}^{N_\Omega} A_i^p(t) \int_{\Omega_h} \nabla \Psi_i \cdot \nabla \Psi_j \, d\mathbf{x} \\ &\quad + K_p \left(\sum_{k=1}^{N_\Gamma} a_k^p(t) \int_{\Gamma_h} \psi_k \Psi_j \, d\mathbf{s} - \sum_{i=1}^{N_\Omega} A_i^p(t) \int_{\Gamma_h} \Psi_i \Psi_j \, d\mathbf{s} \right), \\ \sum_{k=1}^{N_\Gamma} \frac{da_k^p}{dt} \int_{\Gamma_h} \psi_k \psi_h \, d\mathbf{s} &= \int_{\Gamma_h} g_p(a_1^1, \dots, a_{N_\Gamma}^1, \dots, a_1^n, \dots, a_{N_\Gamma}^n) \psi_h \, d\mathbf{s} \\ &\quad - d_p \sum_{k=1}^{N_\Gamma} a_k^p(t) \int_{\Gamma_h} \nabla \psi_k \cdot \nabla \psi_h \, d\mathbf{s} \\ &\quad - K_p \left(\sum_{k=1}^{N_\Gamma} a_k^p(t) \int_{\Gamma_h} \psi_k \psi_h \, d\mathbf{s} - \sum_{i=1}^{N_\Omega} A_i^p(t) \int_{\Gamma_h} \Psi_i \psi_h \, d\mathbf{s} \right), \end{aligned}$$

for $j = 1, \dots, N_\Omega$ and $h = 1, \dots, N_\Gamma$. The above equations can be written, in compact matrix-vector form, as

$$\begin{aligned} \mathbb{M}^\Omega \frac{d\mathbf{A}^p}{dt} &= -\sigma_p \mathbb{M}^\Omega \mathbf{A}^p - D_p \mathbb{K}^\Omega \mathbf{A}^p + K_p (\mathbb{J} \mathbf{a}^p - \mathbb{H}^\Omega \mathbf{A}^p), \\ \mathbb{M}^\Gamma \frac{d\mathbf{a}^p}{dt} &= g_p(\mathbf{a}^1, \dots, \mathbf{a}^n) I - K_p (\mathbb{M}^\Gamma \mathbf{a}^p - \mathbb{J}^\Gamma \mathbf{A}^p) - d_p \mathbb{K}^\Gamma \mathbf{a}^p, \end{aligned}$$

for $p = 1, \dots, n$, where I is the identity matrix

B.2 Temporal discretisation

The above spatial semi-discrete weak formulation requires the solution of $2n$ coupled systems of ordinary differential equations. We set a time step $\tau > 0$, look for the solutions at the time points $t_k = t_{k-1} + \tau$, with $t_0 = 0$, and apply a finite difference scheme. Let $\mathbf{a}^{p,k}$ be an approximation of $\mathbf{a}^p(t_k)$. Therefore, by replacing the time derivatives by their first order difference operator (for example), we aim at solving the following system on the surface

$$\begin{aligned} (\tau^{-1} \mathbb{M}^\Gamma + d_p \mathbb{K}^\Gamma) \mathbf{a}^{p,k+1} &= \tau^{-1} \mathbb{M}^\Gamma \mathbf{a}^{p,k} + g_p(\mathbf{a}^{1,k}, \dots, \mathbf{a}^{n,k}) I \\ &\quad - K_p (\mathbb{M}^\Gamma \mathbf{a}^{p,k} - \mathbb{J}^\Gamma \mathbf{A}^{p,k}), \end{aligned}$$

for $p = 1, \dots, n$. The above temporal discretisation scheme is known as IMEX, because the diffusion terms are considered implicitly and the reaction terms explicitly [47, 36]. The explicit treatment of the reaction terms constitutes a way of obtaining a linear system of equations. By solving the above systems we get the solution of the surface equations at time t_{k+1} . To obtain the solution of the bulk equations at time t_{k+1} we solve the following systems

$$(\tau^{-1}\mathbb{M}^\Omega + D_p \mathbb{K}^\Omega + K_p \mathbb{H}^\Omega + \sigma_p \mathbb{M}^\Omega) \mathbf{A}^{p,k+1} = \tau^{-1}\mathbb{M}^\Omega \mathbf{A}^{p,k} + K_p \mathbb{J} \mathbf{a}^{p,k+1}, \quad (42)$$

for $p = 1, \dots, n$. By taking advantage of the linear reactions in the bulk, and having already calculated the surface solutions at t_{k+1} , we can solve the bulk systems fully implicitly.

C Amplitude equations up to order 3 for $\ell = 4$

$$\begin{aligned}
\dot{A}_0 = & A_0 (\varepsilon - 18 a A_0) + 18 a A_{-1} A_1 + 22 a A_{-2} A_2 \\
& - 42 a A_{-3} A_3 - 28 a A_{-4} A_4 + A_0 (2 c A_{-4} A_4 + (140 b - 2 c) A_{-3} A_3 \\
& + (-600 b + 2 c) A_{-2} A_2 + (320 b - 2 c) A_{-1} A_1 \\
& + (-160 b + c) A_0^2) - 14 \sqrt{10} b A_{-4} A_1 A_3 \\
& - 12 \sqrt{70} b A_{-4} A_2^2 - 14 \sqrt{10} b A_{-3} A_{-1} A_4 + 23 \sqrt{70} b A_{-3} A_1 A_2 \\
& - 12 \sqrt{70} b A_{-2}^2 A_4 + 23 \sqrt{70} b A_{-2} A_{-1} A_3 + 21 \sqrt{10} b A_{-2} A_1^2 \\
& + 21 \sqrt{10} b A_{-1}^2 A_2 + \mathcal{O}(\|\mathbf{A}\|^4),
\end{aligned} \tag{43}$$

$$\begin{aligned}
\dot{A}_1 = & A_1 (\varepsilon - 18 a A_0) + 12 \sqrt{10} a A_{-1} A_2 - 2 \sqrt{70} a A_{-2} A_3 \\
& - 14 \sqrt{10} a A_{-3} A_4 + A_1 ((-28 b + 2 c) A_{-4} A_4 + (273 b - 2 c) A_{-3} A_3 \\
& + (-313 b + 2 c) A_{-2} A_2 + (383 b - 2 c) A_{-1} A_1 + (-160 b + c) A_0^2) \\
& - 210 b A_{-4} A_2 A_3 + 14 \sqrt{10} b A_{-3} A_0 A_4 + 45 \sqrt{7} b A_{-3} A_2^2 \\
& - 40 \sqrt{7} b A_{-2} A_{-1} A_4 - 23 \sqrt{70} b A_{-2} A_0 A_3 + 90 \sqrt{7} b A_{-1}^2 A_3 \\
& - 42 \sqrt{10} b A_{-1} A_0 A_2 + \mathcal{O}(\|\mathbf{A}\|^4),
\end{aligned} \tag{44}$$

$$\begin{aligned}
\dot{A}_2 = & A_2 (\varepsilon + 22 a A_0) - 6 \sqrt{10} a A_1^2 + 2 \sqrt{70} a A_{-1} A_3 - 6 \sqrt{70} a A_{-2} A_4 \\
& + A_2 ((-168 b + 2 c) A_{-4} A_4 + (343 b - 2 c) A_{-3} A_3 \\
& + (-208 b + 2 c) A_{-2} A_2 + (313 b - 2 c) A_{-1} A_1 + (-300 b + c) A_0^2) \\
& - 70 \sqrt{7} b A_{-4} A_3^2 + 210 b A_{-3} A_1 A_4 - 24 \sqrt{70} b A_{-2} A_0 A_4 \\
& - 90 \sqrt{7} b A_{-2} A_1 A_3 + 20 \sqrt{7} b A_{-1}^2 A_4 + 23 \sqrt{70} b A_{-1} A_0 A_3 \\
& + 21 \sqrt{10} b A_0 A_1^2 + \mathcal{O}(\|\mathbf{A}\|^4),
\end{aligned} \tag{45}$$

$$\begin{aligned}
\dot{A}_3 = & A_3 (\varepsilon + 42 a A_0) - 14 \sqrt{10} a A_{-1} A_4 - 2 \sqrt{70} a A_1 A_2 \\
& + A_3 ((-448 b + 2 c) A_{-4} A_4 + (203 b - 2 c) A_{-3} A_3 \\
& + (-343 b + 2 c) A_{-2} A_2 + (273 b - 2 c) A_{-1} A_1 + (-70 b + c) A_0^2) \\
& + 140 \sqrt{7} b A_{-3} A_2 A_4 - 210 b A_{-2} A_1 A_4 + 14 \sqrt{10} b A_{-1} A_0 A_4 \\
& + 45 \sqrt{7} b A_{-1} A_2^2 - 23 \sqrt{70} b A_0 A_1 A_2 + 30 \sqrt{7} b A_1^3 + \mathcal{O}(\|\mathbf{A}\|^4),
\end{aligned} \tag{46}$$

$$\begin{aligned}
\dot{A}_4 = & A_4 (\varepsilon - 28 a A_0) + 14 \sqrt{10} a A_1 A_3 - 3 \sqrt{70} a A_2^2 \\
& + A_4 ((-448 b + 2 c) A_{-4} A_4 + (448 b - 2 c) A_{-3} A_3 \\
& + (-168 b + 2 c) A_{-2} A_2 + (28 b - 2 c) A_{-1} A_1 + c A_0^2) - 70 \sqrt{7} b A_{-2} A_3^2 \\
& + 210 b A_{-1} A_2 A_3 - 14 \sqrt{10} b A_0 A_1 A_3 - 12 \sqrt{70} b A_0 A_2^2 \\
& + 20 \sqrt{7} b A_1^2 A_2 + \mathcal{O}(\|\mathbf{A}\|^4).
\end{aligned} \tag{47}$$

D Plots of the L^2 -norm of transient solutions

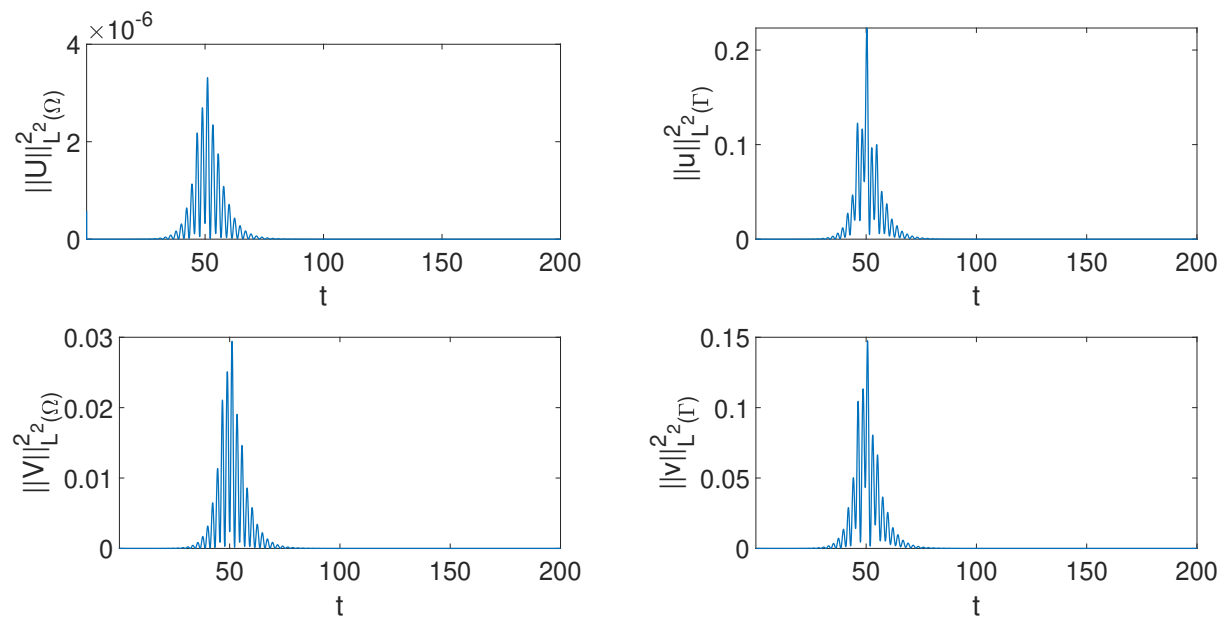


Figure 8: Brusselator for $\ell = 1$.

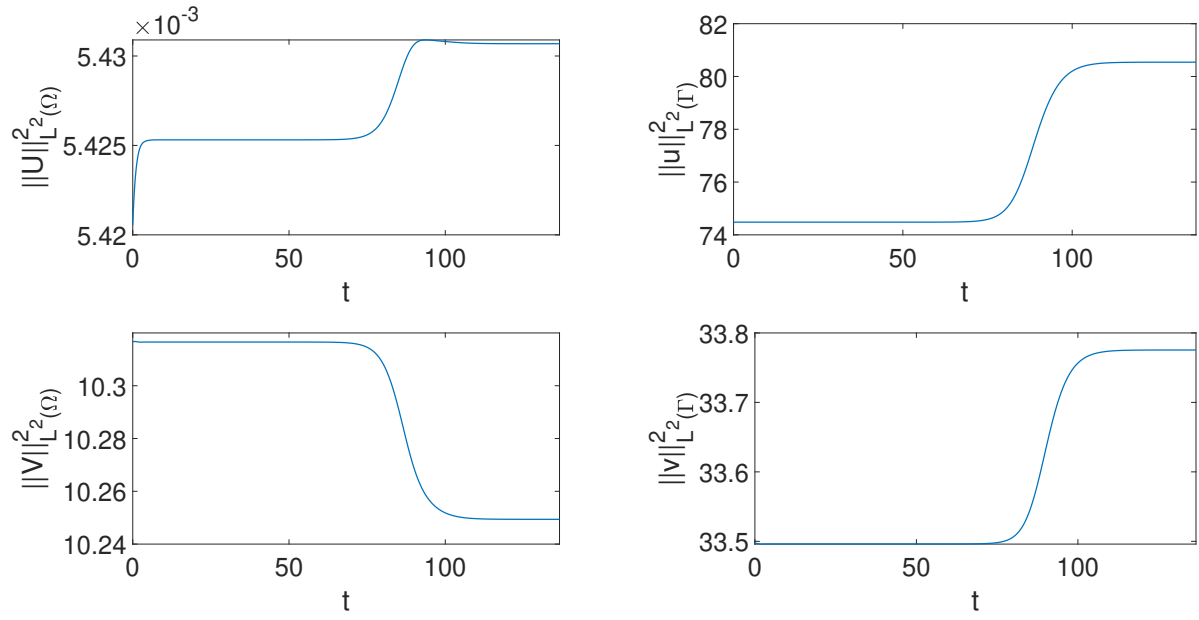


Figure 9: Brusselator for $\ell = 2$.

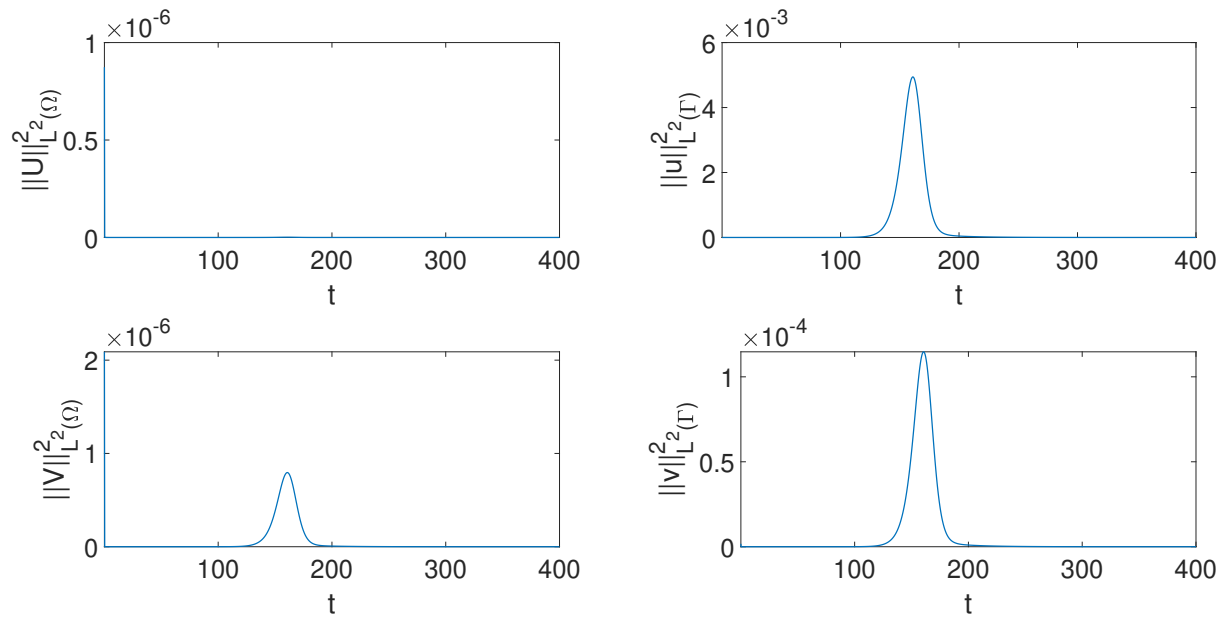


Figure 10: Brusselator for $\ell = 3$.

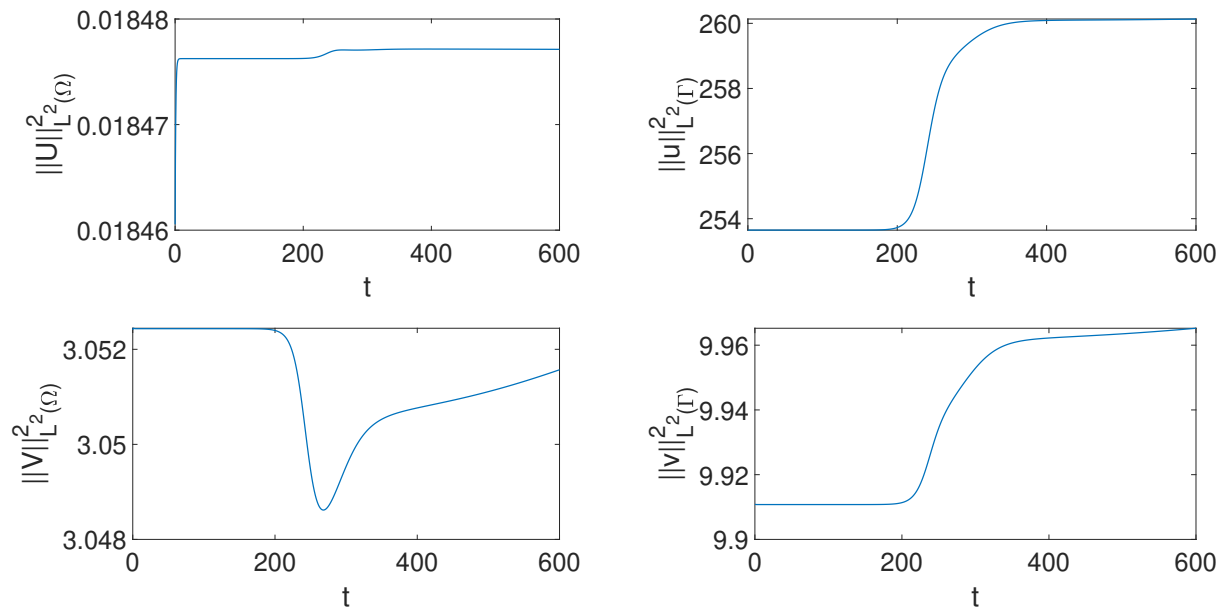


Figure 11: Brusselator for $\ell = 4$.

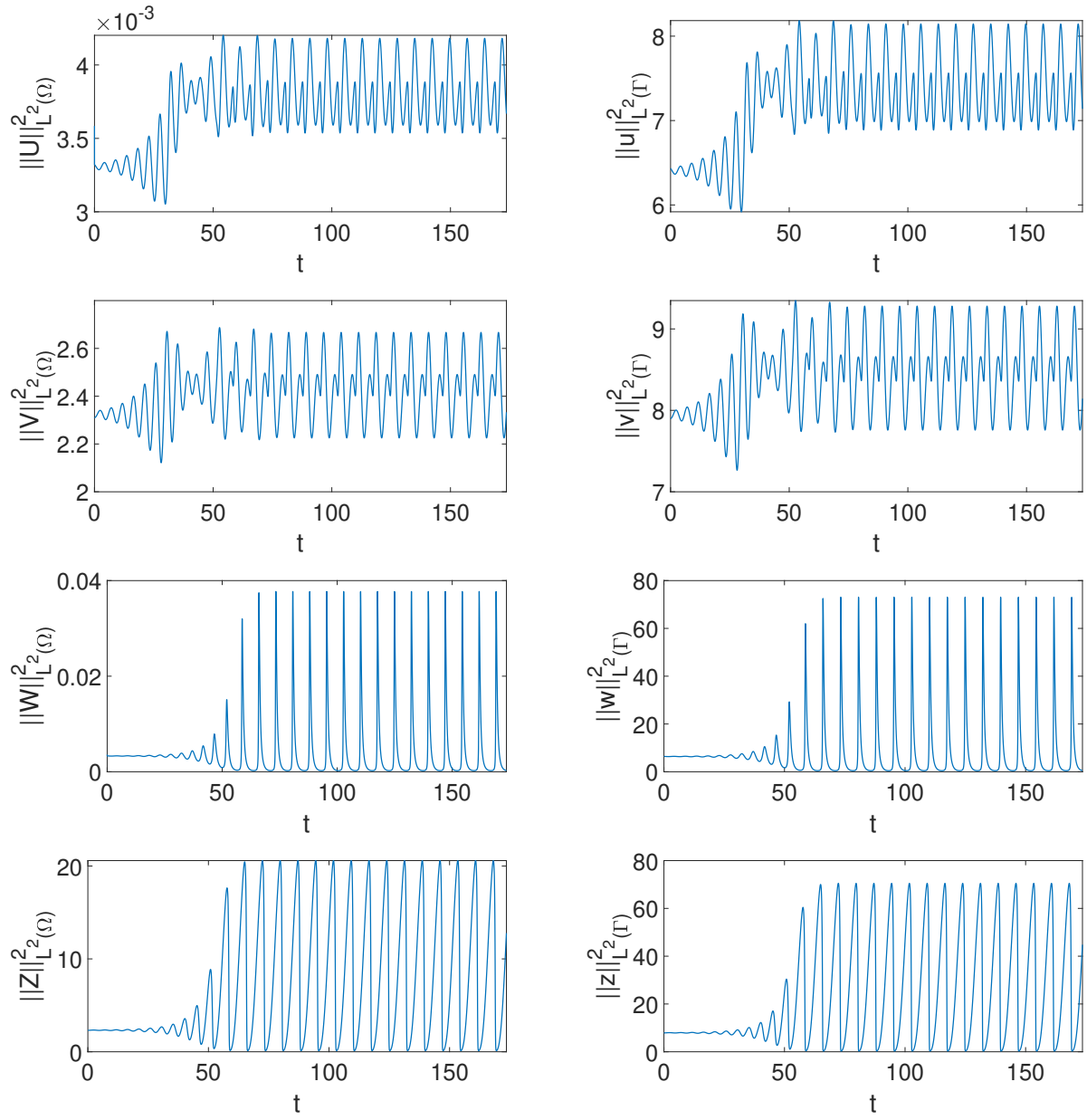


Figure 12: Cell-polarity model for $\ell = 1$.

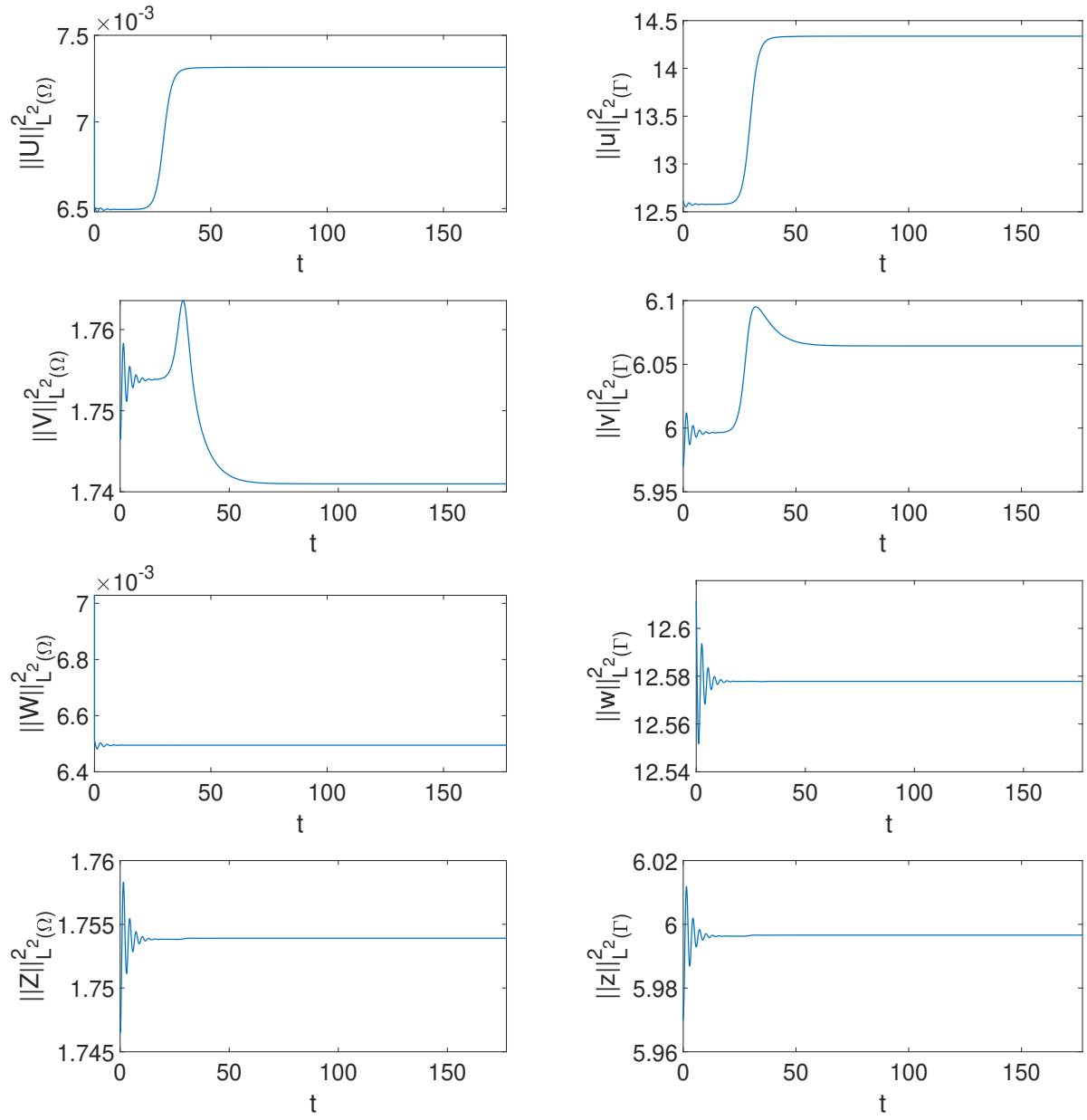


Figure 13: Cell-polarity model for $\ell = 2$.

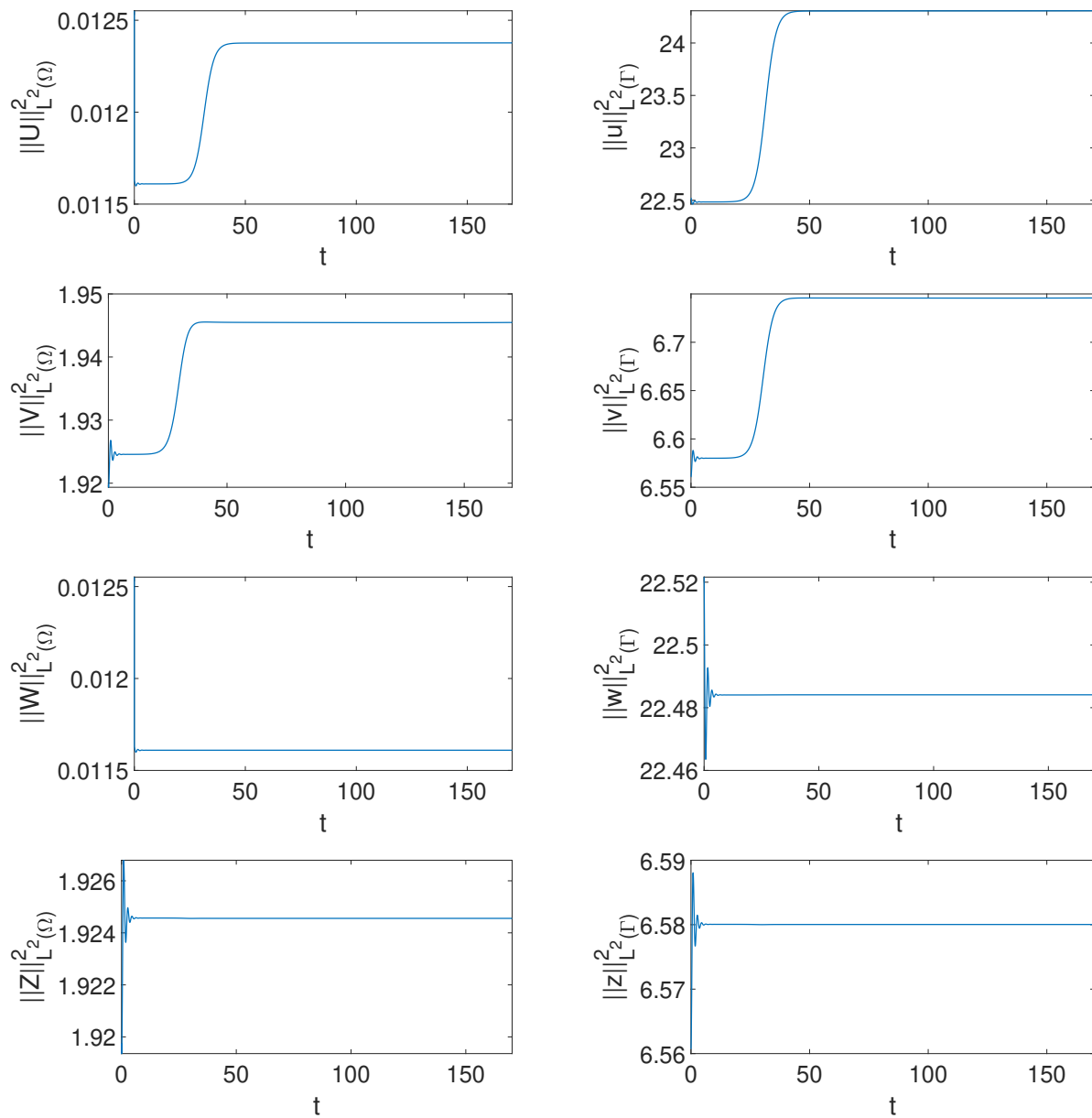


Figure 14: Cell-polarity model for $\ell = 3$.